MEASUREMENTS OF INITIAL VELOCITY IN MATRIX ASSISTED LASER DESORPTION/IONIZATION (MALDI) AND IDENTIFICATION OF WHEAT VARIETIES USING MALDI-TOF.

By

Marek Stephan Znamirowski

A Thesis
Submitted to the Faculty of Graduate Studies
In Partial Fulfillment of the Requirements
For the Degree of

Master of Science

Department of Physics and Astronomy
University of Manitoba
Winnipeg, Manitoba, Canada

August 2004

THE UNIVERSITY OF MANITOBA

FACULTY OF GRADUATE STUDIES

*****

COPYRIGHT PERMISSION

MEASUREMENTS OF INITIAL VELOCITY IN MATRIX ASSISTED LASER DESORPTION/IONIZATION (MALDI) AND IDENTIFICATION OF WHEAT VARIETIES USING MALDI-TOF.

BY

Marek Stephan Znamirowski

A Thesis/Practicum submitted to the Faculty of Graduate Studies of The University of Manitoba in partial fulfillment of the requirement of the degree

Of

MASTER OF SCIENCE

Table of Contents

ACKNOWLEDGMENTS

I would like to thank Dr. Werner Ens and Dr. Ken Standing for their support, advice and guidance in directing the research described in this thesis, as well as the opportunities given to me from my time here in the TOFMA lab.

I would also like to thank and the many other people who have helped me in the process of completing my degree, such as Vic Spicer, who helped tremendously in the computational works in this thesis.

I would like to thank the many colleagues and people I've met in this lab, especially alexandra jilkine, who made my studies here a very enjoyable and memorable experience.

Chapter 4 presents work done for the Canadian Grain Commission, and I would like to thank them for their support and the opportunity to perform research for them.

Finally, I would like to thank my family for their patience and support in the completion of my degree.

ABSTRACT

The results of initial velocity measurements of matrix and analyte in the MALDI plume, and, wheat variety identification by the gliadin spectrum using MALDI-TOF, and are reported. A reflecting Time-of-flight mass spectrometer with delayed extraction (Manitoba TOF II) was used for both measurements of the discussed experiments.

Information on the initial speed of MALDI ions can provide more clues to the nature of the MALDI process, as well as give corrections to *m/z* for linear instruments. Previous initial velocity results showed a discrepancy of values between different methods used. The results here using a technique based on delayed extraction in a reflecting TOF instrument found an average initial velocity of 660 m/s for proteins, and velocities higher than 1000 m/s for matrix ions. These results are consistent with earlier measurements made by a simpler DC technique where ions are desorbed into a field free region prior to acceleration. These results do not correspond to a previous experiment using delayed extraction to measure initial velocities. That experiment did not use a mirror to preserve peak resolution as ours did. The velocity values of the previous delayed extraction experiment were approximately a factor of two lower than the field free and the ones presented here, suggesting possibly a source of systematic error was present in that experiment.

Grain identification is a critical factor in the exportation of grain from Canada. Current methods of identification rely on a kernel visual distinguishability (KVD) grading system which is essential a system where visual characteristics are used to

identify different classes. This method is subjective and dependent on subjective evaluation from individuals. Another set of methods for identification involve gel-electrophoresis or HPLC, but these methods are more time consuming. Grain identification by MALDI-TOF proposes to improve both speed and impartiality of the process. Promising results for identification using MALDI-TOF are given here, used on four Canadian Wheat Classes with a total of seventeen wheat varieties, as well as investigation into the effects of environment of identification. The effects of environment on the wheat spectra seems minimal, and the differences between different wheat varieties were readily identifiable in the MALDI spectra collected.

Chapter 1

Introduction

Mass spectrometry provides qualitative and quantitative information on the atomic and molecular composition of inorganic and organic materials. For close to a century it has grown from a research tool for basic physics to a powerful analytic tool which can provide useful data for many branches of science, from physics and chemistry to oceanography and space science. In 1912 J. J. Thompson showed the fundamental principles of mass spectrometry (i.e. production, separation and recording of the mass of an ionized particle[1]). Two isotopes of neon, masses 20 and 22, were found using a magnetic deflection instrument. The first precision mass spectrometers were constructed by J. Dempster in 1918 [2] and by F. W. Aston in 1919[3], to measure the relative abundances of some isotopes.

Until 1940, the mass spectrometer was used for the analysis of gases and for the mass determination of the stable isotopes of chemical elements[4]. It was later used to carry out quick and accurate analyses of complex mixtures of hydrocarbons from petroleum fractions. When it was demonstrated that a complex molecule could give rise to a well defined and reproducible mass spectrum, interests in the application of mass spectrometry to the determination of organic structures was established.

Since that time, one general goal in the development of organic mass spectrometry has been to investigate larger and larger masses. The requirement of volatilization of samples for such ionization methods as electron impact causes problems when the sample molecules are involatile or thermolabile, that is, when the temperature at which they evaporate is higher than that at which they decompose. Organic compounds, too, are involatile either because their molecular mass is too large or because they are highly polar, as in the case for peptides and proteins.

One of the most successful methods to produce large molecular ions is by bombarding a solid surface, covered with organic molecules, with ions, neutral particles, or photons. The development of desorption/ionization methods for large involatile organic molecules began with particle induced desorption. The application of particle bombardment to produce molecular ions from nonvolatile organic materials was first reported in 1974 by Macfarlane and Torgerson [5] using fission fragments from ^{252}Cf, that is, using high-energy particles of mass ~100 Da and energy of ~100MeV. Early experiments produced molecular ions desorbed from bulk samples of biomolecules with molecular mass close to 2000 Da [6]. The technique was named plasma desorption mass spectrometry (PDMS) because of the plasma associated with a fission fragment as it interacts with matter.

Over the next ten years, the mass range was extended and resolution improved in PDMS by depositing the samples on various type of substrates. In 1984 molecular ions of mass greater than 20 000Da were observed with a conducting target foil [7], and by 1989, Jonsson *et al.* [8] had dramatically improved the mass spectra and mass range using proteins absorbed onto the polymer substrate nitrocellulose. Subsequently, intact

molecular ions have been desorbed up to about 45 000 Da in mass.

Production of ions by fission fragment bombardment couples naturally with time-of-flight mass spectrometry (TOF-MS). Since the introduction of the TOF principle for mass separation of a pulsed ion packet in 1946 [9], the use TOF mass spectrometry has been limited by relatively poor resolution in comparison to other mass spectrometers, like, for example, sector instruments. However PDMS avoids two of the problems previously associated with the limited resolution of TOF-MS. Firstly, from the fission process, one of the recoiling fragments may be used to give a well defined start signal (start time), with the acceleration field of the TOF-MS instrument at a high, stable DC potential, instead of being pulsed. Secondly, the ions are ejected from a solid equipotential surface; thus the energy and spatial spread is much smaller than for traditional gaseous ion sources.

Soon after the discovery of PDMS, another form of particle-induced desorption using low energy ion bombardment emerged. The use of low-energy ion bombardment for desorption of organic molecules was pioneered by Benninghoven in 1976 [10] and was regarded as an unexpected development of static secondary ion mass spectrometry (SIMS) where primary ion impact energies are around a few keV with low ion currents ($\sim$nA/cm^2). The low primary ion currents, in turn, produced low secondary ion currents. The secondary ion currents also decrease with increasing size of molecular ions. Thus, Benninghoven, using a sector-field instrument, was limited in mass range to biomolecules of a few hundred u because of the transmission losses and losses due to scanning the mass spectrum.

An increase in the observable mass range of SIMS was achieved by coupling

SIMS to a TOF instrument, taking advantage of the high sensitivity and mass range of TOF-MS, as had been demonstrated with PDMS. In 1981 Chait and Standing [11] developed a low-energy pulsed ion gun with 5keV Cs+ ions which induced desorption of molecular ions of mass around 1300 Da [12]. The largest polypeptide observed with this technique, using nitrocellulose as a substrate, is cytochrome C with mass about 14 000 Da [13].

In 1982, an increase in the observable mass range in SIMS was also finally achieved on sector-field instruments by using samples dissolved in a viscous liquid like glycerol [14], and using primary ion currents typical of dynamic SIMS (currents greater than $\sim 10^{-5} A/cm^2$), and orders of magnitude higher than in static SIMS. Because the beam consisted of neutral particles [15,16], this technique was named fast atom bombardment (FAB). It is well suited for coupling to existing sector-field and quadropole spectrometers. The neutral primary beam is unaffected by extraction fields near the target, and because it provides sustainable secondary ion currents by the renewal of the liquid matrix surface. Typically FAB analysis is used up to a mass-range of a few thousand Da [17,18].

The final desorption method to be discussed, and which is most relevant to this thesis, involves using a pulsed laser beam as opposed to particle bombardment. In 1976, the use of a nanosecond pulsed laser, together with TOF-MS, was first used to study biological material [19]. The early work on laser desorption mass spectrometry (LDMS) was reviewed in detail by Conzemius and Capellen in 1980 [20] and more recent laser desorption work has been reviewed by Hillenkamp in 1983 and 1985 [21,22].

For about ten years following this development, the first application of laser des-

orption (LD) to biological molecules relied on the absorption of photon energy in the sample molecules themselves. This restricted the types of molecules that could be analyzed; for analysis by UV lasers, this typically required the presence of tryptophan in polypeptides. More importantly, fragmentation restricted the application to rather small peptides, less than about 1000Da [21,22]. However, in 1985, where we find the first reference to 'MALDI', Karas and Hillenkamp found that by mixing the analyte with a suitable organic matrix (initially nicotinic acid to absorb the laser energy), and then illuminating the dried mixture with a laser pulse, it is possible to produce intact molecular ions of a much wider range of samples [24]. The mass range in the initial experiments was limited by detection efficiency in the mass spectrometer, but shows molecular ions from melittin at mass 2.8 kDa. In 1988, after including the energy, intense signals from bovine serum albumin (~66 000Da) were shown, revolutionizing the field [23,25]. Since then, the method has rapidly grown with the discovery of new matrices [26,27], extending the method to other classes of samples (for example, glycopeptides, carbohydrates and nucleotides), with masses in the range of several hundred thousand daltons [28] routinely analyzed. This technique is referred to as matrix-assisted laser-desorption/ionization, or MALDI.

In MALDI, a matrix - usually a small organic acid - is combined in large molar excess with the biomolecule analyte (peptide, protein, etc.). The molar ratio is typically 1,000 - 10,000. Generally the matrix used absorbs UV light very well, and the sample is hit with bursts of laser light a few nanosecond in duration. Most of the energy of the light is absorbed by the matrix, and thus prevents unwanted fragmentation of the analyte.

The matrix undergoes a rapid phase change producing a rapidly expanding plume of gas, resulting in intact gas phase sample molecules and ions. The ions are subsequently accelerated in an electric field and enter a flight tube. The time of flight for the ions is recorded, and the mass of the ions can be thus determined.

At about the same time that MALDI was introduced, another method of producing gas-phase ions from large molecules was developed. In electrospray ionization "ESI" gas-phase ions are produced in atmosphere directly from solution by an electric field applied at the tip of a capillary. The ions are introduced to the mass spectrometer through a small orifice or a capillary separated from vacuum by a few stages of differential pumping. In contrast to MALDI, in which low charge states are produced (typically < 3) ESI produces a distribution of highly charged molecular ions. Compared to MALDI, ESI is more sensitive to contaminants and produces more complex spectra. On the other hand, since a mass spectrometer measures the *m/z* ratio, a modest *m/z*-range quadrupole mass filter, well-suited to a continuous ion source, can be used to measure large proteins. ESI is mentioned here as general background information but the experiments described here do not involve this ionization technique directly.

These latter two ionization methods (MALDI and ESI) have revolutionized mass spectrometry of large molecules. These methods have increased the mass range for some classes of compound (notably proteins) into the range of several hundred kDa, making mass spectrometry a realistic alternative to more traditional methods of molecular weight determination such as gel electrophoresis.

In this thesis, two experiments involving MALDI are described. One is a fundamental study of the initial velocities of matrix and analyte ions to attempt to reconcile some discrepancies in the literature. Knowledge of these initial velocities give better corrections to mass measurements in axial TOF systems, as well as providing clues into the nature of the MALDI process itself. The method used to find initial velocities involved delayed extraction from the desorption region and the use of an electrostatic mirror, details of which will be discussed in Chapter 3.

The second experiment was a feasibility study of applying MALDI-TOF (with delayed extraction) for identifying Canadian wheat varieties from the mass spectral pattern of their gliadin proteins. Four classes of wheat were used, with sixteen varieties examined. Further study into the effects of environment on the gliadin spectra were done as well to examine how the location where the wheat was grown would affect the identification process.

Chapter 2.

Time of Flight Instrumentation

2.1 Time Of Flight Mass Spectrometers

The TOF mass spectrometer operates on the simple principle that a packet of ions, if rapidly accelerated to the same kinetic energy, will possess individual velocities dependent on their *m/z* ratio; if z=1 for all ions, the dependence is essentially with respect to mass. When the ions are projected into a field-free drift region, they will separate according to their mass; the light ions, having a higher velocity, will arrive at the end of the drift space before the heavier ions, which have lower velocity. For ions accelerated to the same energy, the time of flight (TOF) is given by $t=L(m/2qV)^{1/2}$, where L is the length of the flight path and qV is the energy of the ion.

The use of the TOF principle for mass separation of a pulsed ion packet was first suggested by Stephens in 1946 [29], and two years later such an apparatus, called an ion 'Velocitron', was reported by Cameron and Eggers [30].

TOF instruments have several advantages over other spectrometers for analyzing biological molecules:

1) They have no theoretical mass limit, and the only mass limitation is due to

desorption and detection capabilities.

2) The resolution is limited only by the metastable decay, the initial energy spread, and the isotope distribution; this is an advantage at high mass and therefor for biological molecules.

3) The whole spectrum can be examined at one time because no scanning of the spectrum is involved; this improves the sensitivity and the speed of recording.

4) An open geometry, giving much higher sensitivities than those of magnetic sector spectrometers.

To utilize TOF separation in a mass spectrometer, the ions must be formed at the same location and time in the source and pulsed into the flight tube. Matrix assisted laser desorption/ionization (MALDI) is an intrinsically pulsed process, where ions are produced by irradiation of a sample with a beam from a pulsed laser. The laser provides the start pulse, so the coupling to a TOF instrument is a natural one. Each packet of ions reaching the detector at the end of the flight tube will result in a series of detector outputs at various arrival times; these give information concerning the mass of the ions being detected, while the amplitude of the signal in analog mode is a measure of the corresponding ion abundance. Thus a complete mass spectrum is generated for each incident laser pulse.

The most obvious defect of the simple model given above is its failure to take account of the initial energy that the ion possesses as it leaves the target. Variations in the initial energy may give rise to a considerable spread of times of flight, and thus to a deterioration in resolution. However, a modification to the instrument that alleviates this problem is the introduction of a reflector or ion mirror [31]. As illustrated in Fig 2.1., ions

on a plane surface (the 'object plane') just outside the source region have a distribution of velocities. Ions travel freely from this surface until they enter a uniform retarding electrostatic field (an ion mirror). Ions follow parabolic paths within the mirror and leave it with the ion velocity component parallel to the mirror axis (v_z) reversed.

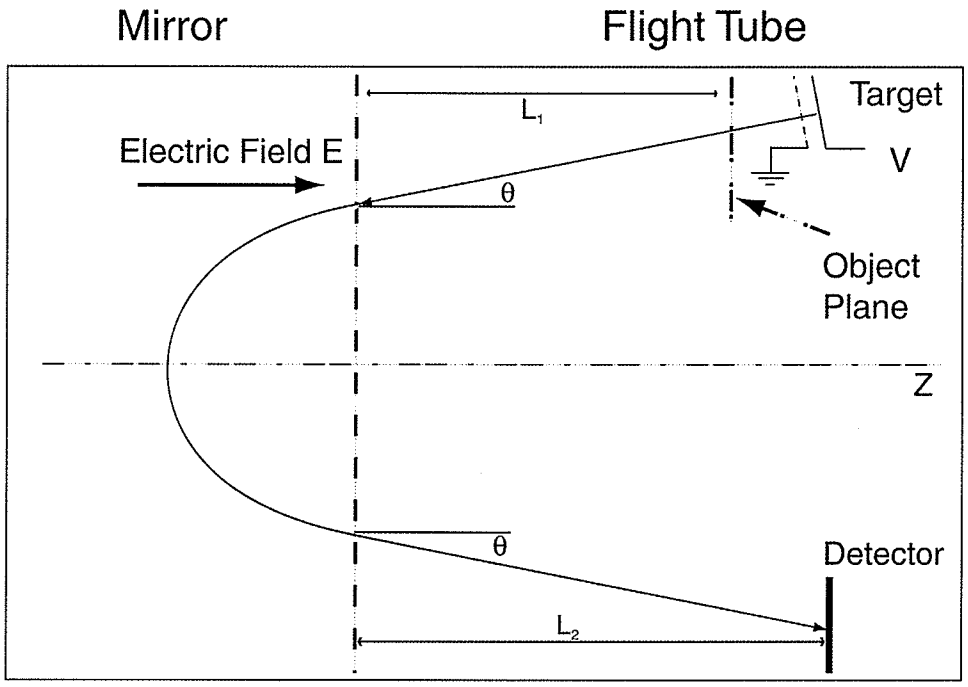

Fig 2.1. Time of flight with electrostatic mirror.

The ion then travels freely to the detector. For $L = L_1 + L_2$, the time spent in free flight is L/v_z, and the time spent in the mirror is $2mv_z/qE$, where E is the magnitude of the retarding electric field. If $v_z = v_0 + \delta$, we can expand as a function of (δ/v_0) to give a total time of flight, as given in equation 1:

$$t = \left(\frac{2mv_0}{qE} + \frac{L}{v_0}\right) + \left(\frac{\delta}{v_0}\right)\left(\frac{2mv_0}{qE} - \frac{L}{v_0}\right) + \ldots$$

Setting $2mv_0/qE = L/v_0$, or $E = 2mv_0/qL$ removes the first order term in δ/v_0. Thus the reflector eliminates the effect of a velocity variation δ to first order. This correction to first order by the reflector does not include the acceleration region, where a spread in the ions' initial energy will have a small effect on the time of flight of the ions.

In the delayed extraction method, ions are produced in pulses (as in MALDI)[1] and then some velocity compensation for ions with different initial velocities occurs in the acceleration region. In this technique a delay is introduced between ion production and the application of the accelerating fields, during which the ions drift freely. For a MALDI source, the ions start with nearly zero spatial spread, i.e. with a pure velocity spread. When the accelerating field is applied, the ions will be separated in space according to their velocity. Those ions with higher initial v_z, will be closer to the end of the accelerating region, and will receive a smaller accelerating impulse. If the time delay and the amplitude of the accelerating voltage are adjusted properly, ions of the same mass will arrive at a focal plane at approximately the same time.

For optimal geometry and resolution, these two methods can be combined together to compensate for each method's limitations, where delayed extraction can correct for the velocity spread of the ions in the source region, but not for the spread that the ions undergo once they pass the acceleration region, while the mirror corrects for velocity differences for ions from the focal plane just outside the acceleration region.

2.2 Manitoba Tof II

All experiments were performed using a reflecting time-of-flight instrument designed and constructed at the University of Manitoba (TOF II). A schematic is shown in Fig 2.2.

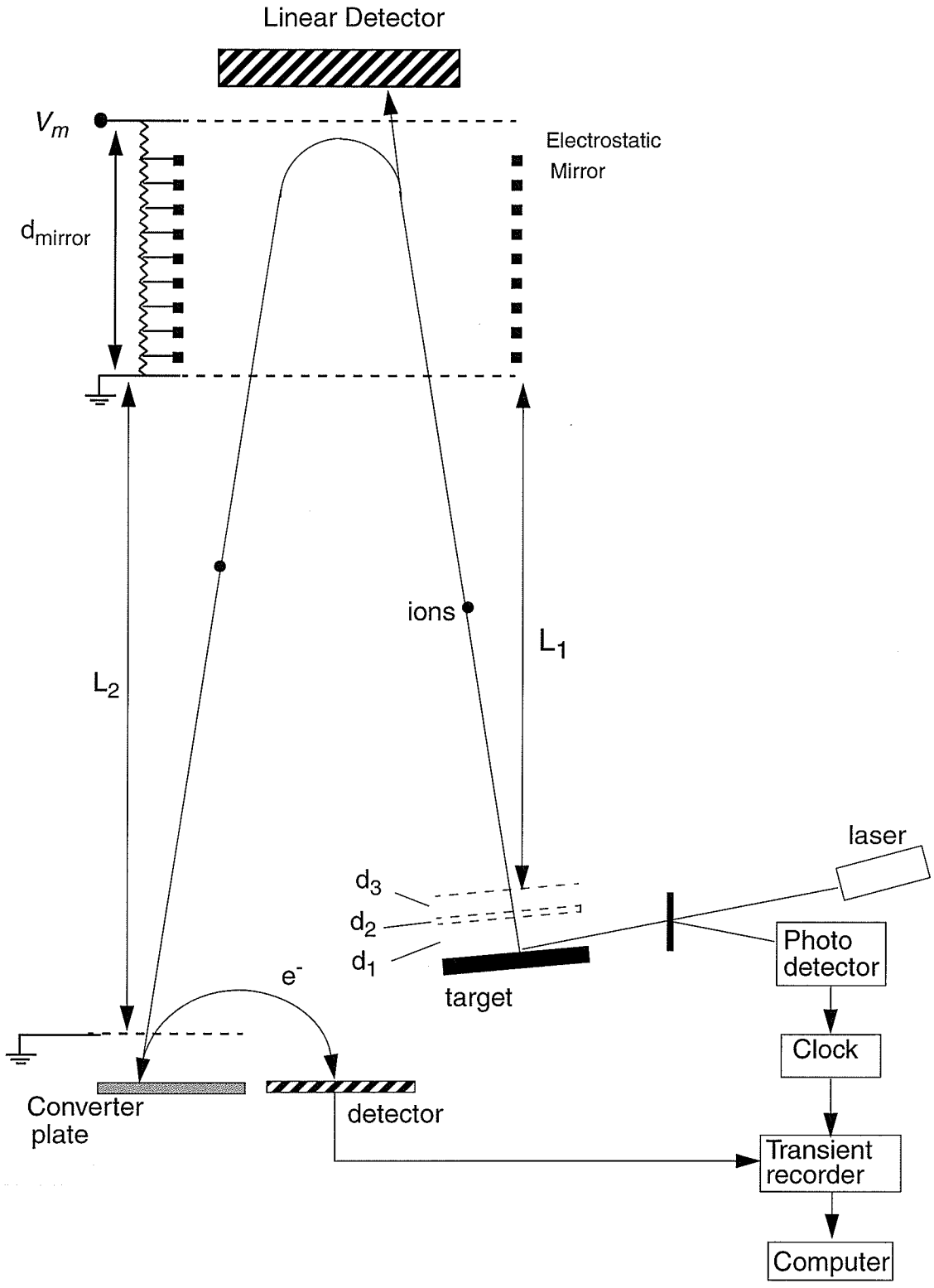

Fig 2.2. TOF mass spectrometer used for measurements of initial velocities [83]

The Manitoba TOF II is a reflecting TOF mass spectrometer with capabilities for linear operation. It was used in positive ion mode as an analytical tool for research into grain identification and "initial" velocity measurements in UV-MALDI. In the research for grain identification, the linear mode was used, while research in initial velocity measurements used the reflecting mode.

OPTICS: The target was irradiated with a N_2 laser (ND337: Laser Science, Inc., Cambridge, MA, USA) with a wavelength of 337nm and a pulse duration of about 3 ns. This instrument is configured to allow two different angles of incidence (77 degrees and 20 degrees) as shown in Fig 2.3. At a glancing angle of incidence (77 degrees) the laser beam was coupled into a 1 m long, high-temperature fiber (F-MCC-T: Newport, Mississauga, ON, Canada) The dimensions of the fiber are 250 microns for the coating diameter, and 200 microns for the core. A homogeneous intensity profile at the other fiber end face is formed because of multiple reflections of the laser beam inside the fiber. The surface of the fiber tip is then imaged 1:1 onto the target by two planoconvex lenses, the laser incident first on a lens with ($f = 15\text{cm}$) and then on one with $f = 30cm$ arranged in infinite conjugation. At this glancing angle the laser light passes behinds the grids and hits the target directly, as shown in Fig 2.3.

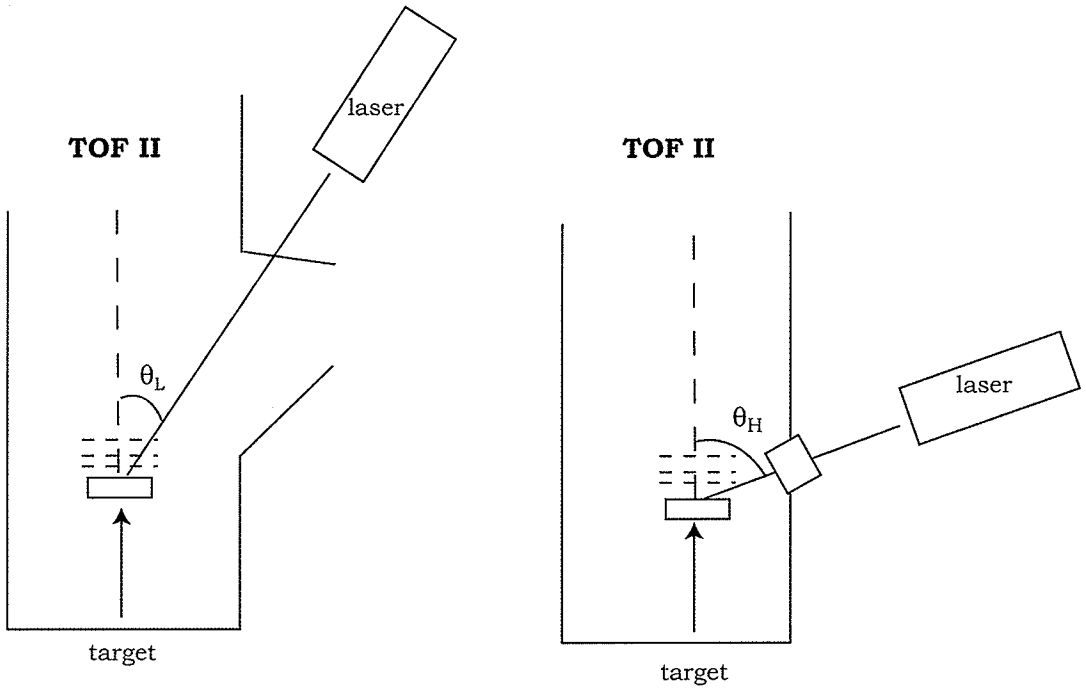

Fig 2.3. Angular configurations for Tof II

At the more normal angle of incidence (20 degrees), a fiber was not used, and the laser was reflected directly off a front silvered mirror through the same arrangement of planoconvex lenses as described above. In this case, the UV laser light had to travel through the three grids above the target, and was reduced in intensity by the percentage transmission of each grid and an increased amount of fluence was needed for ion generation. This increase in fluence needed precluded the use of a fiber optic cable at this near normal angle. The focal point was not precisely at the target plane, but a few mm away from it for an increase in the ion yield detected.

Instrument geometry: The field-free drift lengths are L_1 = 0.51 m, and L_2 = 0.70 m, and for the mirror length is d_{mirror} =35 cm. In linear mode, the total length is 1.16 m. In reflecting mode, ions spend equal time in the mirror and in free flight, so the effective flight path is $2(L_1 + L_2)$ = 2.42 m. The distances between target and first grid, first grid and second grid, and the second grid and grounding grid are d1 = 6.223 mm, d2 = 1.994 mm, and d3 = 9.475 mm respectively. In the usual setup only one middle grid is used. A second middle grid, electrically connected to the first was added to help screen the electric field for the velocity measurements, as described in Chapter 3.

The first and second grids used were 200 lines/inch Ni with 78% transmission, while the grounding grid was 70 lines/inch Ni with 90% transmission.

Mirror: The ion mirror is made of non-magnetic stainless steel. It consists of two end plates and 28 rings (8.79 mm thick, 11.75 cm inner diameter) spaced 3.25 mm apart using ceramic balls and has a length of 34.9 cm between the two grids on the end plates. The angle between the spectrometer axis and the ion path is approximately 1.4 degrees, to allow the ions to hit the detector at the bottom of the instrument.

Detection: Ion detection for both top and bottom was done using an electron converter plate and two microchannel electron multiplier plates in a chevron configuration, as in Fig. 2.4. The electron converter plate is coated with a thin film of CsI to perhaps enhance electron conversion efficiency due to the low work function. The conversion dynode is maintained at a high negative potential and a 90% transmission grid is at ground potential to provide for post-acceleration of positive ions into the dynode and the acceleration of the secondary electrons away from the dynode. The distance

from the grid to the dynode is 2mm, and a typical negative voltage of 800 - 1.45 kV was placed on the dynode for the detection of positive ions.

The magnetic field for bending the electrons is produced by a pair of rectangular coils separated by 11 cm and mounted outside the vacuum chamber. The center-to-center separation of the conversion dynode and the microchannel plate is 6 cm, so the electrons travel through a semicircular path with a radius of 3 cm.

For each detector, two microchannel plates (as shown in Fig 2.4.) with 4 cm diameter effective area are separated by a 250 mm stainless steel ring and mounted 1mm from a stainless steel collector. The front surface of the first plate is usually at ground, and a typical potential difference of 800 V was applied to each plate, and 200 volts was placed between the second plate and the collector. For the top detector, the voltages were supplied by a voltage divider mounted outside the vacuum chamber. For the bottom detector, the resistance of the microchannel plates was used as the voltage divider. The resistance across one microchannel plate is 40 MΩ, and provides the proper voltage divide for the plates to function. An electron gain of ~10^7 is achieved in this configuration and the output pulse has a rise time of ~0.5 ns and a pulse width of 1.5 ns.

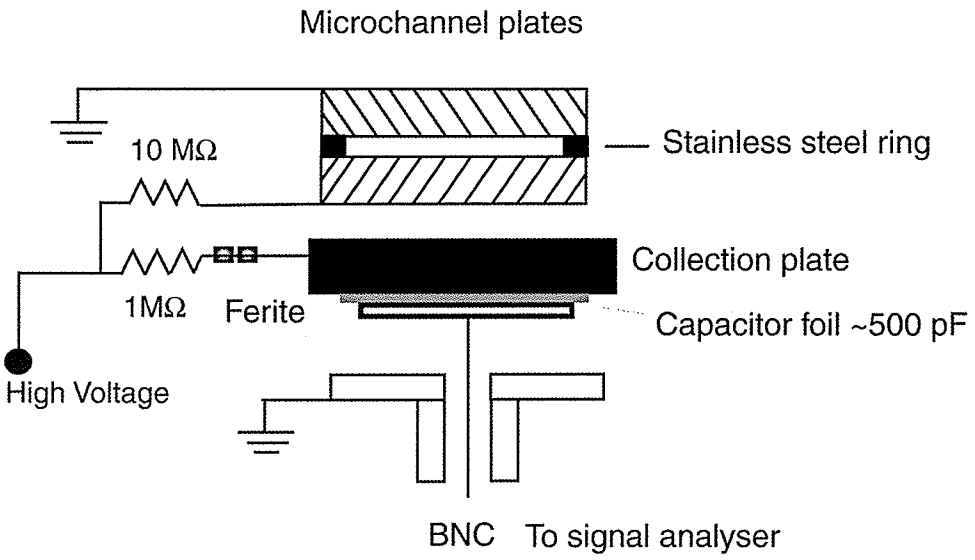

Fig. 2.4 Microchannel plate configuration used for detecting reflected ions

Data Acquisition: The pulse was then monitored by the Lecroy oscilloscope and communicated to the computational system (Supermac c600 603e/200 OS 8.6) using a GPIB/SCSI interface (IOTech MacSCSI488: IOTech Inc. Cleveland, OH, USA). Signal processing was done with in house software (TOFMA).

A photodetector triggered by a partial reflection of the laser beam (Scientech Model 301-020 high speed photodetector, 1 ns resolution) was used to trigger electronics associated with data acquisition. The signal from the photodetector was used to trigger the delay generator and set the start time for spectra acquisition. This was fed into a pulse discriminator (Ortec Constant-Fraction Discriminator, model 473 A) with a walk of < +/- 200 ps. The measured time difference between input/output for this setup was 100 ns. The CFD pulse was then signaled into a delay generator (Princeton applied research, model 9650A) which triggered both the start time for the time of flight recorded by the

transient recorder (Lecroy TR8828D) and the start of the voltage pulse. The delay pulse was given to a Fast high voltage transition switch (Behlke HTS300) which was used to switch the pulse voltage generated by a power supply (Spellman Model MP40P24)

In DC operation constant voltages V_1 and V_2 are applied to the target and the electrically connected middle grids, with the final grid at ground. The middle grids are at an intermediate voltage, but can also be placed at ground.The time of flight for the ions is measured from the time a partial reflection of the laser hits the photodetector to the time the ions are detected on the microchannel plates. All ions gain the same energy and separate in their time to reach the detector over the free flight region, with the time of flight corresponding to the mass of the ions., as shown in Fig 2.5.

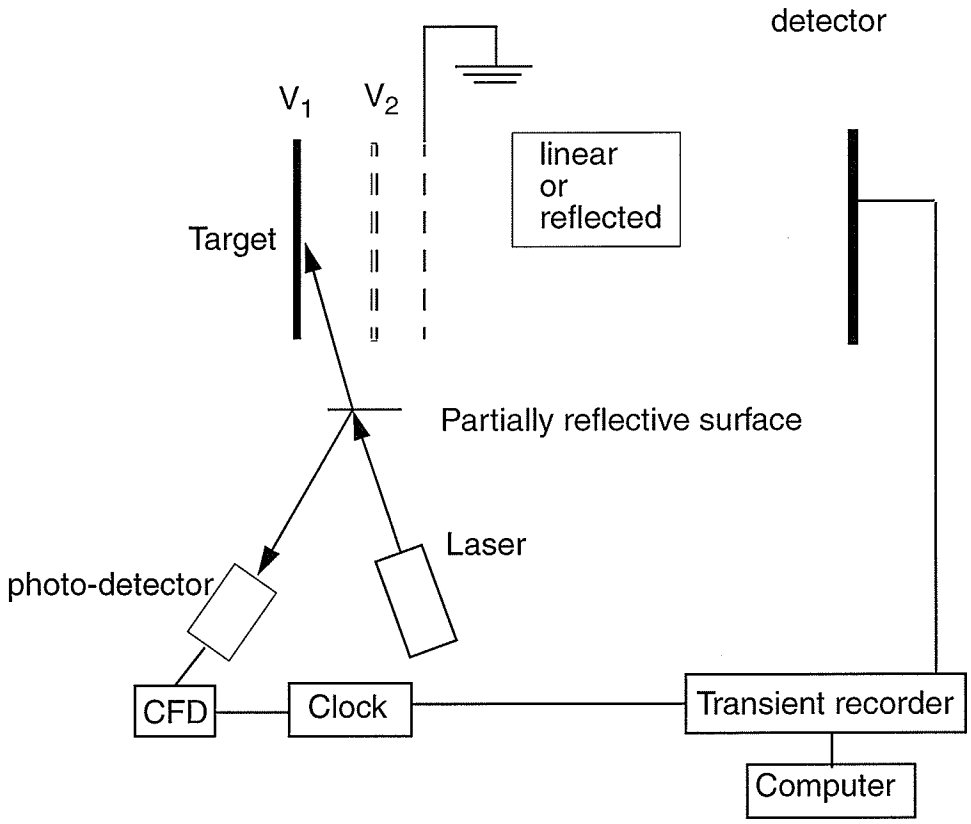

Fig 2.5. DC timing schematic for Tof II

In delayed extraction, the target and middle grids are set to the same initial potential, with the final grid still at ground, as shown in Fig.2.6. The ions generated by the laser pulse are allowed to drift between the target and the first grid for a time τ, (the delay time) at which point the voltage of the target plate is increased, and the ions undergo acceleration. This method is primarily used to give better resolution to the time of flight spectrum by partially correcting for the initial velocity distribution of ions in the MALDI plume.

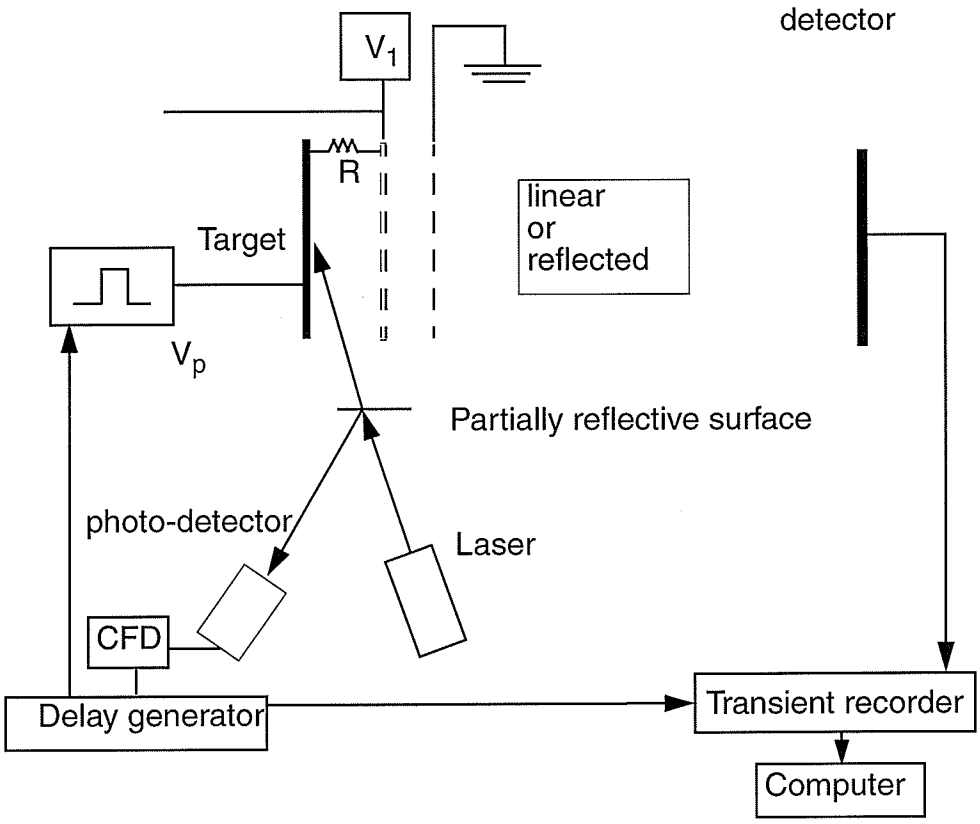

Fig 2.6. Delayed extraction timing schematic for Tof II

Chapter 3.

Measurements Of Initial Velocity In MALDI

3.1 Introduction

The discovery of MALDI (matrix assisted laser desorption/ionization) by Karas and Hillenkamp [24,25] led to a dramatic extension of mass range and sensitivity in the mass spectrometric analysis of proteins. The ejection dynamics of the ion production process have an important influence on the mass spectrum in time-of-flight measurements. Measurements of initial time and velocity spreads contribute to the understanding of the ejection mechanism, and provide information relevant to the design and performance of the mass spectrometer. Several experimental measurements of initial velocity distributions in matrix-assisted laser desorption have been reported. [32-48].

The field-free method: The study by Beavis and Chait at Rockefeller University [35] was the first to measure the velocity distributions of large ions ejected into a field-free region, and subsequently accelerated. Previous measurements were dominated by effects of the extraction field [42]. In the Rockefeller measurements, a two-stage, gridded acceleration stage is used, and the spectrum is measured with and without a field in the first region. The difference in time-of-flight of selected ions corresponds to the drift time of the ions in the first field-free region and indicates the initial velocity. These measurements showed that all polypeptide molecular ions above about *m/z* 5000 produced by matrix assisted laser desorption at the ion production threshold fluence have a similar velocity distribution, with an average velocity of 750 m/s. On the other hand, higher velocities were measured for smaller peptides, and for the matrix ions (sinapinic acid, *m/z* 224), which gave a mean initial velocity of 1140 m/s.

Similar results were subsequently reported by other groups [38,43,44]. Measurements in this laboratory (Verentchikov. et al [38]) previous to this work, found somewhat lower velocities of ~ 500 m/s for molecular ions with mass higher than about 5000 Da. In addition, the measurements also showed that the initial velocities of large protein ions were independent of laser fluence. More recent measurements in our laboratory using an orthogonal geometry also give velocities in the same range [40].

As mentioned, in contrast to the initial velocity measurements of higher mass ions, measurements of initial velocities for smaller species yield somewhat inconsistent results, although the measurements all indicate that the velocity increases with lower mass and higher fluence [38]. In particular, Spengler found that with the laser focused to a 10 μm diameter spot on a single crystal of DHB (2,5-dihydroxybenzoic acid M=137) with 1 and 6 times the threshold irradiance, ions were desorbed with mean velocities from 2700 to 7400 m/s. [43]. The increase in initial velocity with decreasing mass was not observed for desorption of neutrals [49-51]. The different behavior of light ions is not surprising since they are more sensitive to the effects of space charge and of penetrating fields than heavy ions.

The delayed-extraction method: The introduction of delayed extraction to improve resolution in a TOF instrument [52], provided an alternative method to measure initial velocities, as demonstrated by Juhasz et al. [53]. In this method, the first acceleration region is field free when the laser pulse strikes the sample; an extraction pulse is then applied after a time delay τ. Juhasz *et al.* showed that, to a good approximation, the time of flight in a linear instrument is linear with τ and the slope depends on the initial velocities, and thus measurements of the time of flight of the ions as a function of the delay time yield the average initial velocity. However, in contrast to the field free method [35], in which the initial axial velocity distribution is extracted, the delayed extraction method yields only the mean value of the axial velocities.

The initial velocity values for bovine insulin (m/z 5733.5) were measured by the delayed extraction method to be 300-350 m/s for a large variety of matrices (alpha-cyano-4-hydroxycinnamic acid {alpha-CHCA}, sinapinic acid, 2-(4-hydroxypheny-lazo)benzoic acid {HABA}, 2-thiohydantion) and in the range of 500 m/s for some others (2,5-dihydroxybenzoic acid {sDHB}, 3- hydroxypicolinic acid {3-HPA}). These results, and subsequent results from Karas et al. using the same method and same instrument [54] are substantially different from those obtained using the field free drift time method. For example, insulin desorbed from sinapinic acid gave results in the range of 500-750 m/s in the field free method, a factor of almost 2 times higher than the results by the delayed extraction method. Similarly, the matrix velocities were also found to be higher in the delayed extraction method than in the field free method.

Understanding the discrepancies: Resolving the discrepancy between the results from these two methods is the goal of the present experiment. The field-free method is more straightforward, and relies on simpler principles and assumptions, but it has been difficult to identify a single factor in the delayed extraction method that can account for a factor of two in the measured velocities. Nevertheless, there are several plausible contributions to an explanation which we identify below; some are considered in greater detail later.

Time scale:

One possible explanation is related to the different time scales involved in the two experiments. Both experiments make the assumption that the ions leave the target with the initial velocity v0 which is unchanged until the extraction pulse is applied. In reality, the ions interact with the expanding gas plume and presumably the larger ions take some distance and some time to be accelerated via collisions to their full velocity. This time is not well-known, but it can be reasonably assumed that plume interactions are not significant after a few hundred nanoseconds, since very sharp peaks can be obtained with time delays of this order. In the field-free method, the assumption of instantaneous acceleration is reasonable, since the velocity is measured over approximately 10 μs. However, in the delayed extraction measurements made by Juhasz, the velocity measurement is completed in 600 to 800 ns [53], so the acceleration time may be significant. The delay times used in the delayed extraction experiment cannot be arbitrarily increased, because the mass resolution is optimum for a single value of the delay, and degraded resolution at longer times makes it increasingly difficult to evaluate the peak position. The length of the delay time is also limited by the time it takes for the ions to reach the first grid. In fact, to avoid non-uniform field effects, the extraction pulse should trigger well before the ions are in the proximity of the first grid.

Field penetration:

Both the field-free method and the delayed extraction method rely on a field-free region at the sample target separated from a strong extraction field by a highly

transparent conducting mesh. Unfortunately, as described in detail below, a grid is not a perfect shield from an Electric field, and the penetrating field can significantly perturb the measurements. The penetrating field can be largely eliminated by applying a compensation voltage to the grid as was done by Juhasz et al. [53], but it is difficult to determine the correct value [56].

Incident Angle:

Experiments by LeBeyec et al suggest that the MALDI plume is directed back in the direction of the incident laser beam [55]. This means that the axial component of the velocity measured by both methods described above decreases as the angle of incidence becomes more glancing. In order to explore the effect of the angle on delayed extraction measurements, the experiment was performed using two incident angles, 20° and 77°. Because the shape of the laser profile was much less circular for the glancing angle experiments, precise reproduction of the laser beam profile was not possible in examining ion velocities from two different angles.

* * * * * * * * * *

Recently, since our measurements were completed, Berkenkamp *et al.* [56] performed delayed extraction experiments similar to those of Juhasz et al [53], but in a different geometry, using longer delay times, and with more attention paid to the compensation voltage. The experiment gave initial velocities of protein ions of approximately 700 m/s, consistent with the field-free measurements.

As already mentioned, the primary motivation of this experiment is similar to that of Berkenkamp *et al.* [56], i.e. to reconcile the results from the two methods used to find initial velocities of ions. In our experiments, a longer first acceleration stage was used to allow longer delays, a reflecting geometry is used to preserve the narrow peak widths at long delays, a double-grid is used to minimize field penetration, and two incident angles are used.

3.2 The Delayed Extraction Method (linear TOF)

The principle of the delayed-extraction method of determining initial velocities of ions in the MALDI plume is simplest to introduce with the linear TOF geometry shown in Fig. 3.1. The ions are assumed to leave the sample surface with an axial component of velocity v0 in a field free region; i.e. the target is initially held at the same potential as the middle grid V_g. After a time delay tau, the extraction pulse is applied to the target to increase its potential by V_p, or to a total potential of $V_a=V_p+V_g$. The total time-of-flight is measured from the time the pulse is applied until the ions are detected, and consists of three components: the remaining time spent in the first acceleration region (t_1), the time spent in the second acceleration region (t_2), and the time spent in free flight (t_3).

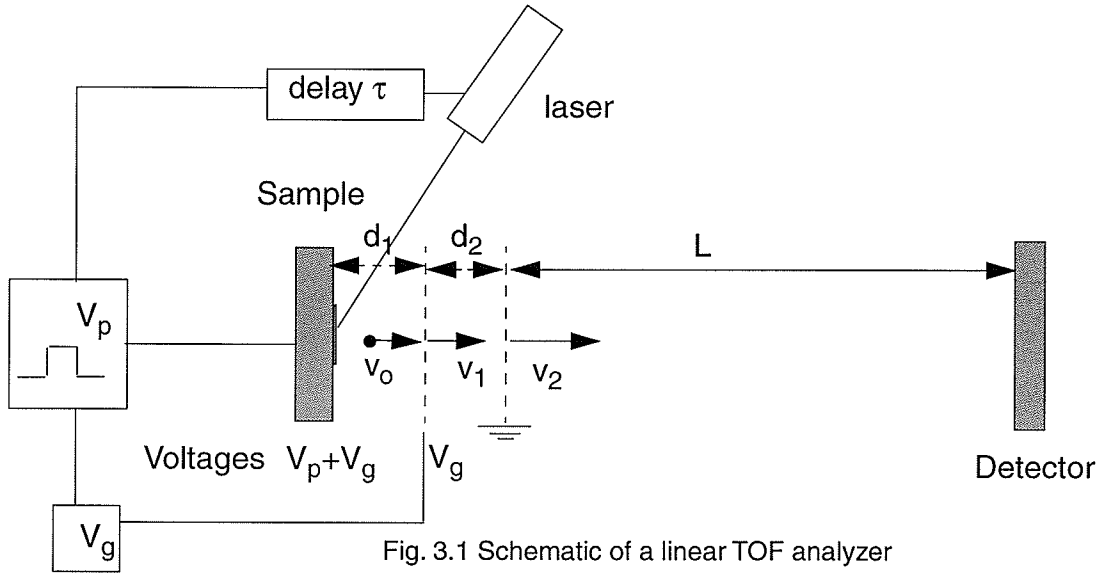

Fig. 3.1 Schematic of a linear TOF analyzer

The basic idea of the method can be understood most easily by neglecting the acceleration time. Then the flight time for an ion of mass *m* is

$$t = t_3 = \frac{L}{v_2} = L\sqrt{\frac{m}{2T_2}} \qquad 3.1$$

where $T_2 = \frac{1}{2}mv_2^2$ is the kinetic energy after the second grid. The kinetic energy clearly depends on the delay τ, since the distance the ion travels in this time ($v_0\tau$) deter-

mines the fraction of the pulsed potential V_p that contributes to the energy:

$$T_2 = \frac{1}{2}mv_0^2 + qV_p\left(1 - \frac{v_0\tau}{d_1}\right) + qV_g = \frac{1}{2}mv_0^2 + qV_a - qV_p\left(\frac{v_0\tau}{d_1}\right)$$

Introducing the nominal velocity of an ion v (the velocity of an ion with zero initial velocity), where $qV_a = \frac{1}{2}mv^2$ and dividing by qV_a gives

$$\frac{T_2}{qV_a} = \left(\frac{v_0}{v}\right)^2 + 1 - \frac{V_p}{V_a d_1}v_0\tau$$

Neglecting the 2nd order in $\frac{v_0}{v}$ and substituting for T_2 in equation 3.1

$$t = L\sqrt{\frac{m}{2qV_a}}\left(1 - \frac{V_p}{V_a d_1}v_0\right)^{(-1)/2}$$

Expanding the square root to first order, and using $qV_a = \frac{1}{2}mv^2$ gives

$$t = \frac{L}{v} + \frac{(V_p/V_a)L}{2d_1}(v_0\tau)$$

which clearly shows the linear dependence on τ. The slope is then given by

$$\frac{dt}{d\tau} = \frac{(V_p/V_a)Lv_0}{2d_1}\frac{}{v}$$

Finally, since the nominal velocity is not known directly, but the time is necessarily mea-

sured, we approximate the nominal velocity with $v = L/t$ giving

$$\frac{dt}{d\tau} = \frac{(V_p/V_a)}{2d_1} v_0 t = \beta v_0 t$$

Thus, measurement of the slope, the voltages V_p and Va, and the grid spacing d1, yields the initial velocity.

A similar but more involved development that takes account of the time during acceleration is given in Appendix A (and in ref [53]), and gives for the constant β

$$\beta = \frac{h}{2d_1 L_e} \qquad with$$

$$h = \frac{V_p}{V_a} L + \frac{2d_2\sqrt{V_p/V_a}}{1+\sqrt{V_p/V_a}} - \frac{2d_1}{\sqrt{V_p/V_a}}$$

$$L_e = L + \frac{2d_2}{1+\sqrt{V_p/V_a}} + \frac{2d_1}{\sqrt{V_p/V_a}}$$

which amounts to an approximate 10% correction.

This linear approximation is better for larger voltage pulses in linear TOF mode. For lower voltages, higher order terms become important, and it may be desirable to fit the exact TOF equations to the data rather than simplify and use the slope [56].

3.3 The Delayed Extraction Method (reflecting TOF)

In a linear geometry, resolution is optimized for a single value of the delay time, and decreases as the delay is changed. This limits the useful range of delays that can be used for determination of initial velocity. Moreover, the delay time must be kept substantially shorter than the time it takes the ions to reach the first grid to avoid non-uniform field effects. In the Juhasz measurements, the delay time was limited to approximately 800 ns [53]. In a reflecting TOF geometry, resolution is less sensitive to the delay time, so longer delay times may be used, while still preserving enough resolution to evaluate the peak centroids.

We have therefore used the reflecting geometry to determine initial velocities with the delayed extraction method. The principle of the method is the same: flight times are measured as a function of the delay time and the resulting dependence is fit to the predicted dependence using the initial velocity as the parameter. However, in the reflecting geometry, the time-of-flight is not a simple linear function of τ, so the exact equation developed using Maple [93] is fit to the data.

The dimensions and potentials are shown in Fig. 3.2.

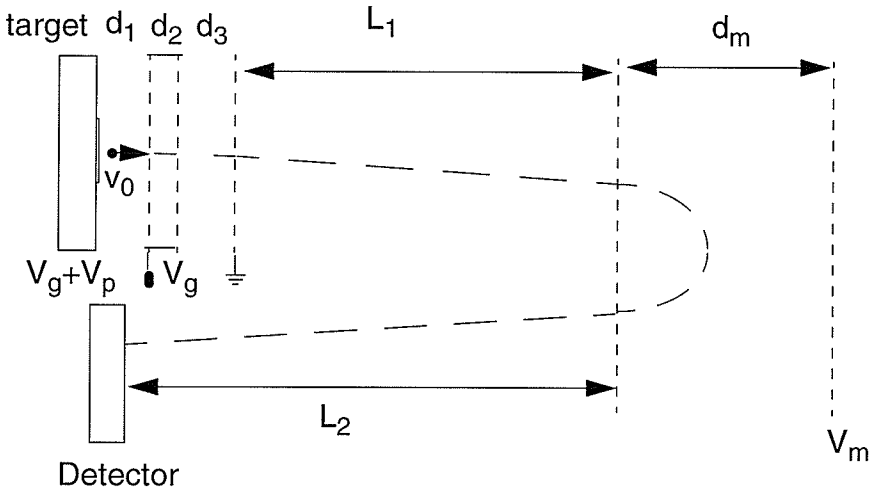

Fig. 3.2 Schematic diagram of reflecting TOF

showing relevant voltages and dimensions

The dimensions are d_1 = 6.223 mm, d_2 =1.994 mm, and d_3 = 9.475 mm, d_m = .349 m, L_1 = .51 m and L_2 = .70 m. The transmissions of the grids are 90% with 200 lines/inch for the ground grid and 78% with 70 lines/inch for the two grids at V_g.

The use of a mirror gave a significant improvement in peak resolution over that of linear experiments where it is typically less than 1000 in the best case and decreases to ~100 for long delays. In our case, the resolution for leucine enkephalin -arg (YAGFLR) was 3980, 1990 and 800 for delay times of 0, 2.8 and 5.6 microseconds respectively, as shown in Fig 3.3.

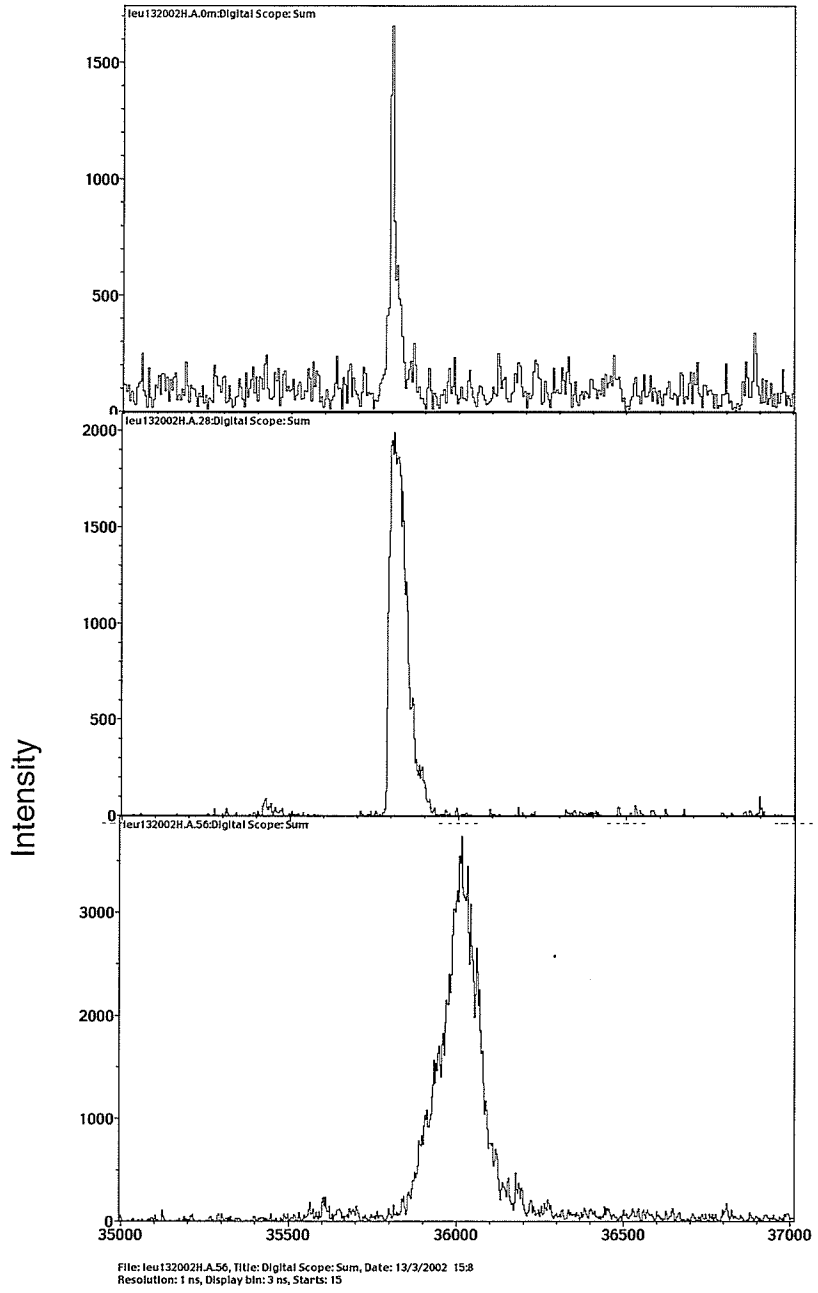

Fig 3.3 leucine enkephalin -arg with 0,2.8,5.6 microsecond delay time

As before, the ions are assumed to leave the sample surface unimpeded with an axial component (z-component) of velocity v_0 in a field-free region. After a time delay τ, an extraction pulse is applied to the target to increase its potential by V_p, or to a total potential of $V_a=V_p+V_g$. The total time-of-flight is measured from the time the pulse is applied until the ions are detected. Here an additional grid is used in the acceleration region to minimize penetrating fields as described in detail in the next section.There are then two new contributions to the total flight time compared to the simple linear geometry described earlier: t_{gap} is the time spent in the gap between the two middle grids, and t_m is the time spent in the mirror. The theoretical flight time is then given by

$$tof(\tau) = t_1 + t_g + t_2 + t_3 + t_m$$

The values for t_1, t_2, and t_3 are the same as for the linear case:

$$t_1 = \frac{m(v_1 - v_0)}{qE1}$$

$$t_2 = \frac{m(v_2 - v_2)}{qE2}$$

$$t_3 = \frac{L}{v_2}$$

Here $L = L_1 + L_2$ represents the total z-component of the free flight path after the acceleration region. As before, v_0, v_1, and v_2 are the axial (z) components of the velocities at the target, first grid, and final grid; E_1 and E_2 are the electric fields between the grids as shown; and m and q are the mass and charge of the ion. The flight time in the gap is simply

$$t_{gap} = \frac{d_2}{v_1}$$

and the time spent in the mirror is twice the time required to stop the ion in a constant electric field E_m:

$$t_m = m\frac{v_2}{qE_m}$$

Again, the velocities can be determined from the respective kinetic energies:

$$T_0 = \frac{1}{2}mv_0^2$$

$$T_1 = T_0 + qV_p\left(1 - v_0\frac{\tau}{d_1}\right) = \frac{1}{2}mv_1^2$$

$$T_2 = T_1 + qV_2 = \frac{1}{2}mv_2^2$$

and the electric fields are simply $E_1=V_p/d_1$, $E_2=V_2/d_2$, and $E_m=V_m/d_m$. With these substitutions, the time-of-flight can be expressed as a function of the initial velocity, the delay time τ, applied voltages, and geometrical constants (see Appendix B). A plot of this calculated time-of-flight as a function of τ for reasonable values of the constants and for initial velocities up to1000 m/s shown in Fig 3.4, reveals an approximately linear dependence over a range of about 4000 ns. However, the deviation from linearity is sufficient that we decided to fit the data to the explicit tof equation, rather than approximate it. For this purpose, it is necessary to introduce a constant time-offset as a fitting parameter. The constant term (zeroth order) in the TOF expression is much more sensitive to the geometrical constants than is the shape of the dependence of the TOF on the delay; thus, as is the case in the linear approximation, the initial velocity is extracted from the τ-dependence, rather than the absolute TOF.

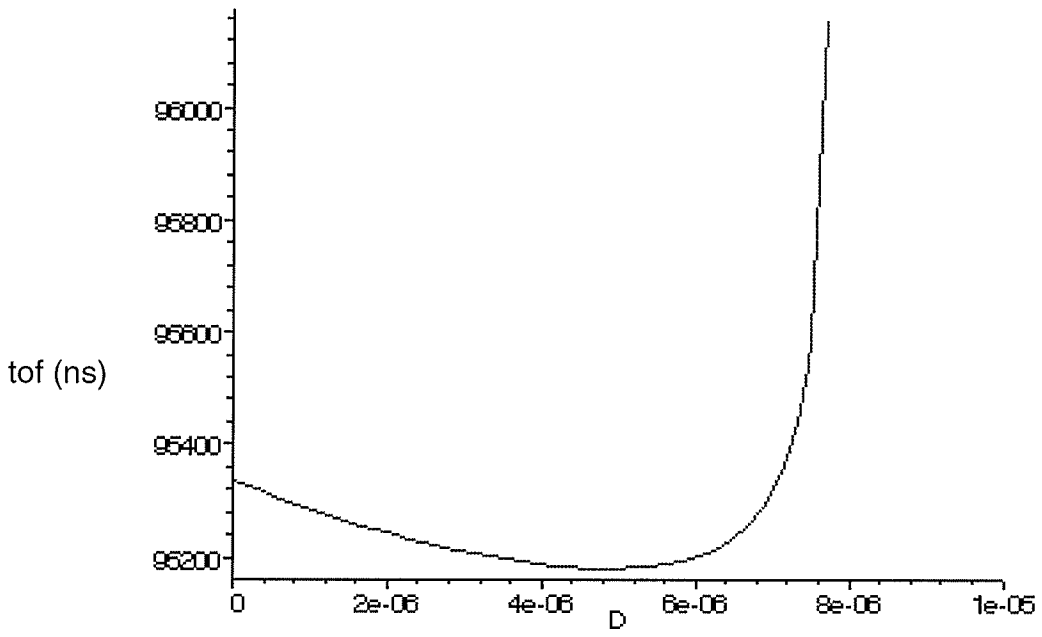

Fig 3.4 Plot of Calculated time-of-flight vs. delay for insulin with an initial velocity of 800m/s

The source dimensions d_1, d_2, and d_3, (see Fig. 3.2) were measured with a micrometer. The mirror length was obtained from previous measurements of the instrument by Tang [57]. The free flight regions were determined from the time of flight of a known mass (insulin at 5734 Da), with dc voltages on the target and mirror. The distance $L = L_1 + L_2$ could then be solved for from the time of flight equation shown above.

As stated in Chapter 2, there is a small angle (1.4 degrees) with which the target is deviated from normal (not shown in schematic). This is to ensure that the accelerated ions travel in the appropriate trajectory to strike the detector after reflection by the mirror. The difference in T_2 between the normal and this angle is less than.03%, and so it was not included in any of the analysis.

Uncertainties in the values of the acceleration voltage, pulse voltage, mirror voltage, and the distances d_1 and d_m are expected to be considerably less than 1%. The effect of these uncertainties on the extracted velocities was examined empirically by comparing the initial velocity of insulin found using one data set and the measured parameters, and the resulting initial velocity if each parameter was changed by 1% and 5%. A 1% change in any of these values resulted in a change in the extracted initial velocity by less than 3%. For a 1% change in the mirror voltage, the time-offset required to fit the data was an unrealistic 500 ns, confirming at least for this parameter, that the uncertainty is much less than 1%. For exaggerated variations in the parameters of 5%, the extracted velocities changed by 15% or less, but in this case the time-offset was significantly higher for each of the parameters. In all the reported fits, the time-offset was less than 100 ns, giving confidence that the errors in the parameters was small. The fluctuation in the extracted velocities from experiment to experiment, due presumably to the physical condition of the sample or laser, was typically 10% - 20%, so the uncertainties in the parameters were ignored

3.4 Effects of Field Penetration

For delayed extraction to be a useful technique for determining the initial velocity of ions, the region between the target and the first grid must be field free during the delay time, otherwise the ions will undergo acceleration due to the residual field present in the region, and the initial velocity will not be correctly identified.

A completely closed conducting cage could remove the influence of one region's field from another region, but in practice grids are often used to allow the transmission of ions. Unfortunately, a grid is not a perfect shield. A common rule-of-thumb suggests the penetrating field is negligible at distances of three times the hole diameter. This can be justified to some extent for a single hole in the shielding electrode, and for considerations of lensing effects (i.e. fields not normal to the plane of the electrode). However, a periodic sequence of holes permits a homogenous field to penetrate as though the grid were a perfect planar electrode with a small offset voltage [58].

Grosser and Schulz have calculated the effect for two conducting plates with a grid electrode between them as shown in Fig. 3.5 [58]. The plane parallel electrodes are at potentials ϑ_α and ϑ_β, and are separated from a by a plane grid at potential ϑ_g by distances h_a and h_b. The grid is assumed to have zero thickness. If $\vartheta_\beta > 0$ and $\vartheta_\alpha = \vartheta_g = 0$, we have the situation described above for delayed extraction MALDI, with ϑ_β the high voltage to be shielded. The average z-component (axial) of the electric field

between the two grounded electrodes is given by

$$\bar{E}(z) = \frac{1}{F}\int_F dr^2(-\partial_z \vartheta(r,z))$$

where $F = L_1 L_2$, L_1 and L_2 being the dimensions of the doubly periodic rectangular unit cell, and r is the radial distance from the centre of the cell.

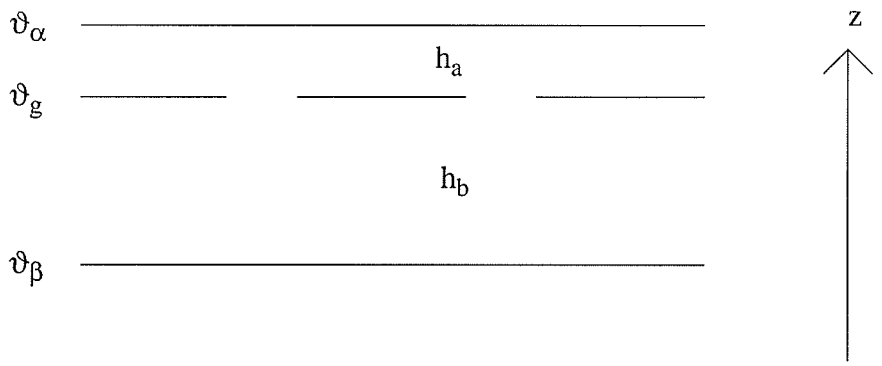

Fig. 3.5 Electrode configuration for the calculation of penetrating field.

The solution to this equation [58] eventually gives an average field consistent with an offset potential $\delta\vartheta$ applied to a plane electrode at the same position illustrated in Fig. 3.6, given by

$$\delta\vartheta = \frac{(E'_2 - E_1')}{\frac{1}{h_a} + \frac{1}{h_b} + \frac{2}{p}}$$

where p is a parameter determined by the grid geometry and has the dimensions of length, and E'_1 and E'_2 are the uncorrected fields $(\vartheta_g - \vartheta_\alpha)/h_a$ and $(\vartheta_\beta - \vartheta_g)/h_b$, respec- (a)
tively. For a a square grid geometry, the value p is given by [58]

$$p = \frac{L}{2\pi}\ln\left(2\frac{L}{\pi B}\right)$$

where L is the distance between two wires (center to center) and B is the wire width.

For 78% transmission p = .0337 mm and for 90% transmission p = 0.143 mm.

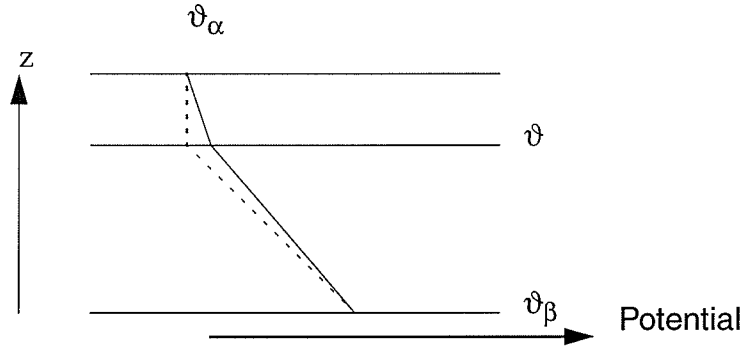

Fig 3.6 Resulting potentials for a perfect intermediate electrode (dashed line) and for a transparent mesh (solid line).

Calculations using these equations showed that for our initial system with a single intermediate grid (90% transmission, 70 lines/inch), the field penetration into the desired field-free region would correspond to an effective grid voltage of approximately 60 volts when a 10kV potential was placed across the middle and grounding grid. This effect can be offset by applying a dc potential to the grid, as mentioned earlier, but depends on an accurate knowledge of the field penetration. Instead, we introduced a second intermediate grid with a finer grid spacing (200 lines per inch with 78% transmission). Equation (a) was applied first to the intermediate grid nearest the grounded grid,

and then the calculated effective voltage on this grid was used to calculate the electric field between the two intermediate grids. The equation was then applied again to calculate the subsequent field penetration between the target and the first grid. This recalculation of field penetrations gave effective offset potentials of 62 volts and 0.6 volts for the two grids. The small field between the grids introduces an effect independent of the delay time, and so is absorbed by the offset time described earlier; the smaller field in the target region is negligible for the present purposes.

The effects of field penetration on the velocities obtained from the fits were calculated for representative cases, and were found to be less than ~1% - substantially smaller than the variation between data sets for the same analyte and matrices, and were therefore not included.

3.5 Sample Preparation

The analytes (bovine insulin 5734 Da, sheep heart myoglobin 169451 Da, and leucine enkephalin -arg 725 Da) were dissolved in a solution of 50% acetonitrile and water plus 0.1% TFA at a concentration of ~1 g/L. Matrix was also dissolved in 50% ACN/ 0.1%TFA until saturated, and 1-2 μL of 10^{-4} M analyte solution was mixed with 10 μL of matrix solution. This mixture (2μL) was then placed on the stainless steel target and allowed to dry in air. For larger crystal formation (near 1 mm in size, such as DHB matrix) a glass slide was used to crush the crystals to a finer state. Other matrices with finer crystal structure were not crushed. Typical sample sizes were ~ 2 mm in diameter.

3.6 Results

Initial velocity measurements were made using the described method for bovine insulin, sheep heart myoglobin, and leucine enkephalin -arg (YAGFLR) using matrices DHB (2,5- dihydroxybenzoic acid), alpha-cyano (alpha-cyano-4-hydroxy-cinnamic acid), and sinapinic acid (3,5-dimethoxy-4 hydroxycinnamic acid).

Examples of data sets used for fitting the initial velocity of insulin and YAGFLR at glancing and near-normal angles are shown in Figure 3.7.

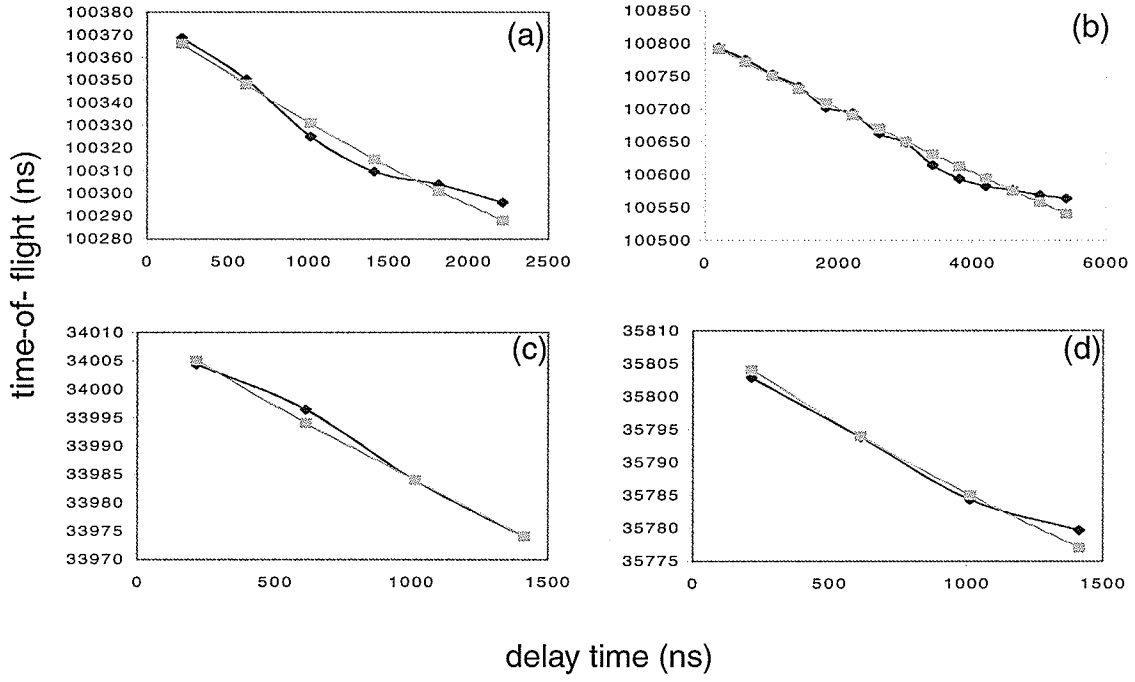

Fig 3.7. Examples of fits used in velocity determination. The lighter points represent the fit, while the darker points are data. The graphs represent the following. (a) insulin in sinipinic at near normal incidence, with a velocity of 670 m/s and a delay range of ~2200ns. (b) insulin in α-cyano at shallow incidence, with a velocity of 580 m/s and a delay range of ~5400 ns. (c) leucine in sinipinic at shallow incidence, with a velocity of 1200 m/s and a delay range of ~1400 ns. (d) leucine in sinipinic at near normal incidence, with a velocity of 1110 m/s and a delay range of ~1400 ns.

Resulting velocities from the parametric fit to the time of flight equations are given below (see Appendix C for fitting routine). In most cases, several velocity fits (up to seven) were made with various pulse and acceleration voltages. Effects of different angles of incidence of the laser, matrix, and masses of analyte ions were examined to search for factors involved in the initial velocities of MALDI ions.

A complete summary of the velocities measured is shown in Table 3.1 (for the more glancing incident angle) and Table 3.2 (for the more normal incident angle).

Table 3.1 Summary of velocity measurements using glancing laser incidence. In cases where more than one measurement was made, all the values are shown with the mean value shown in bold. Based on the fluctuation of the measurements in these cases, we estimate an uncertainty of approximately 15% in the individual results.

Ion (protonated)	**Velocity (m/s)**		
	Matrix		
	αCHCA	DHB	SA
αCHCA	1250		
DHB		1050	
SA			1290
Leu-enkephalin-arg	1340		
	1240		
	1140		
	1140		
	990		
	990		
	1240		
	1150	1230	2000
Insulin	590		
	560	990	
	590	590	
	580	**790**	830
Myoglobin		800	
		880	
		840	

In most cases, several velocity fits were made with various pulse and acceleration voltages. The quality of the fits was generally good in most cases, so the uncertainties reported were established by the variations from experiment to experiment. In the case where 7 separate measurements were made, the standard deviation was about 15%. As is now well established, the results show that the average initial velocities of peptides and proteins above a few thousand Daltons are quite uniform.

Table 3.2. Summary of velocity measurements using near-normal laser incidence. In cases where more than one measurement was made, all the values are shown with the mean value shown in bold. Based on fluctuation of the measurements in these cases, we estimate an uncertainty of approximately 15% in the individual results.

Ion (protonated)	Velocity (m/s)		
	Matrix		
	αCHCA	DHB	SA
αCHCA	1210		
	1480		
	1370		
	1350		
DHB		1250	
SA			1410
Leu-enkephalin-arg		1760	1360
	1380	1580	1780
	1440	1440	1330
	1260	1460	1790
	1360	**1560**	**1565**
Insulin	600		730
			790
	700	410	730
	750	720	490
	680	**565**	**685**
Myoglobin		670	590
		630	470
		650	**530**

Table 3.3 compares our results with those of other groups for representative matrix ions and larger proteins of 5000 Daltons or more. Our measurements for the larger proteins are consistent with the early measurements by Beavis and Chait [35] as well as by other groups [38] who used the field-free method to determine initial velocities, giving initial velocities, with sinapinic acid as the matrix, in the range of 700 m/s. These are in contrast to the measurements by Juhasz et al [53] and Karas et al [94] using the delayed extraction method, which gave velocities almost a factor of two smaller. More recent measurements using the delayed extraction method by Berkenkamp et al. in Münster [56] also give values closer to 700 m/s, suggesting possible systematic errors in the early delayed extraction measurements as outlined in the Introduction.

Table 3.3 Comparison of the present velocity measurements with measurements from other experiments. The protein velocity correspond to average velocities for proteins above about 5000 Da desorbed from sinapinic acid.

Author (year)	Method	Velocity (m/s)	
		DHB	Proteins (SA)
These results (2002)	Delayed Extraction	1250	660
Berkenkamp (2002) [56]	Delayed Extraction	1070	689
Dworschak (1999) [95]	Orthogonal Injection	1800	700
Karas (1999) [94]	Delayed Extraction		332
Juhasz (1997) [53]	Delayed Extraction	396	352
Martens (1994) [38]	Field-free	800	550
Beavis (1991) [35]	Field-free	1140	770

The Münster experiments [56] were made in a linear TOF instrument, but with a different source geometry, allowing delay times similar to ours, up to 6000 ns, although with significantly degraded resolution. Their results show explicitly that plume interactions influence the velocity measurements for delay times less than 1000 ns. The results with the longer delays were similar to field-free measurements made in the same instrument. Indeed, in most cases, the error bars from the two measurements for a given analyte overlap, although the velocities obtained by the delayed extraction method still seem systematically lower by about 10 - 20%. Berkenkamp argued that collisions of (partially) accelerated ions with neutral plume constituents after application of the delayed extraction pulse must be assumed to lead to significant modifications of the final ion velocities. The extent of this energy deficit will be higher the earlier ion acceleration sets in, i.e., the lower the delay time τ [56].

As in the Juhasz measurements [53], the Münster experiments also used a compensation voltage on the intermediate grid to prevent field penetration. The field-free condition was verified in the Juhasz experiments by ensuring the flight time of Na^+ ions had a linear dependence on the delay time. However, Berkenkamp showed that a linear dependence was also observed in a strongly over-compensated case. They therefore used the transition to linearity as the correct compensation voltage. In our case, the two-grid system made this unnecessary.

Velocities of matrix ions are somewhat higher in our experiment compared to most other reports, but these velocities have been shown to be sensitive to laser fluence [38], which is not accurately known in any of the experiments. Measurements in an

orthogonal geometry with higher fluence gave even higher velocities of lighter ions [95]. For the same reason, comparison of velocities of small peptides are of limited relevance, and are not indicated in table 3.3

The measured velocities from the two incident laser angles did not reveal an effect of laser angle within the uncertainties of the experiment. A small effect may be masked by the variations from experiment to experiment, but it does not appear that this accounts for a significant part of the discrepancies mentioned earlier.

3.7 Summary and Conclusion

In this experiment, several changes were made to the delayed extraction method used by Juhasz [53] to try and improve the accuracy of the initial velocities. One change was to use much longer extraction delay times to reduce the influence of plume effects (such as shielding of the ions from the extraction pulse). The best resolution for using delayed extraction occurs only in a small window of delay times for a given set of ion mass, acceleration and pulse voltage. Since the range of delay times used is typically much greater than the range of delay times for optimal resolution, a large reduction of the resolution of the ion peaks would be present for a significant portion of the data set. The experiment was modified, as mentioned previously, with an electrostatic mirror which mostly corrected for this loss of resolution. This is because of the lower sensitivity to non-optimal potential relations between the mirror and the initial acceleration region. A double grid system between the target and grounding grid was employed in this experiment to reduce the penetrating field to negligible levels, with calculations of the residual fields in this setup show previously in this chapter.

In general, the results indicate that higher mass MALDI ions (>5000 Da) have initial velocities between 500-800 m/s consistent with field-free experiments and more recent delayed extraction experiments but substantially higher than reported in the earlier delayed extraction experiments. Lower mass ions (<1000 Da) and matrix ions were desorbed with much higher speed, more than 1000 m/s in most cases.

The effects of the different angles used in this experiment were generally not observable, so, if present, were masked by the uncertainty of the measured initial velocities.

Chapter 4.

Grain Variety Identification Using MALDI-TOF

4.1 Introduction

For purposes of exportation, identification of wheat varieties is necessary for quality control and reliability in the wheat product to match that which it is claimed to be. Some inherent quality characteristics for wheat include protein content, protein quality, hardness, gluten strength, and milling yield. The properties of wheat dough and processing characteristics are determined primarily by the quantitative and qualitative properties of the gluten protein complex. Major protein groups in this complex are monomeric gliadins and polymeric inter-chain disulfide-bonded glutenins [59-62]. Gliadins are a heterogeneous group consisting of more than 100 proteins divided into four subgroups (α,β,γ,ω) based on electrophoretic mobility [63]. Most have molecular masses in the range of 30-40 kDa. The polymeric glutenin proteins, with molecular masses ranging from less than 300 kDa to millions of Da are composed of two groups of subunits. The low molecular weight (LMW) glutenin

subunits are similar in size and structure as the gamma-gliadins (30-40 kDa). The high molecular weight (HMW) glutenin subunits range in molecular mass from 65-90 kDa [64]. The LMW subunits account for most of the mass of the glutenin proteins found in wheat [62, 64].

The Canadian system for grading wheat along with other grains relies on protein fingerprinting in conjunction with visual analysis. For economic reasons there is a critical need to improve upon methods for the grading and/or variety identification of commercial wheat samples at high throughput and in inland terminals. The most common procedure of variety identification involves the separation of the gliadin proteins into bands of different mobility using polyacrylamide gel electrophoresis (PAGE) under acidic conditions [65-68]. Sufficient bands (about 40) are normally available to accurately identify most varieties although closely related varieties may present problems. In the latter case, identification can normally be achieved by two-dimensional electrophoresis or, combinations of electrophoresis with other techniques such as reversed-phase high performance liquid chromatography (RP-HPLC) due to the much higher number of resolved components [69,70].

Other techniques that are applicable to wheat identification based on gliadin protein patterns include RP-HPLC [7] and capillary electrophoresis [71,72]. Although high resolution can be obtained with RP-HPLC, this equipment is considerably more costly to purchase and maintain relative to PAGE and, in contrast to PAGE, can accommodate only one sample per run, which greatly restricts throughput. Recent studies suggest that capillary

electrophoresis may be a viable alternative to PAGE for wheat variety identification [73]. Although the cost of equipment and maintenance is also much higher than PAGE, this method can produce much faster separations (<10 min relative to >1hr for PAGE) and can be automated for sample injection.

For variety mixtures, all of these techniques require single kernel analysis for accurate results. To obtain an accurate variety distribution in bulk samples for grading or certification, a large number of individual kernels must be analyzed. Thus, throughput can be dramatically reduced when this information is required.

MALDI-TOF MS is being widely used to characterize purified, partially purified and complex mixtures of proteins and other macromolecules with masses up to several hundred kilodaltons or more [80-82]. The advantages of the technique include extremely high sensitivity (< 1 picomole), tolerance to impurities, high throughput with automation (< 2 min/sample) and relatively precise (±0.01%) mass determination for proteins with masses <100,000daltons [75,82]. Unlike other MS techniques such as electrospray ionization (ESI), the low charge state in MALDI-TOF-MS results in less complex spectra which facilitates identification of parent ions in partially purified or complex mixtures [75-82].

MALDI-TOF MS has been used to determine the mass of purified wheat α-gliadins [78] and high molecular weight (HMW) glutenin subunits [78,79]. It has also been used to characterize the mass profile of crude or partially purified extracts of wheat gliadins, low molecular weight (LMW) glutenin subunits and HMW glutenin subunits [80-82]. The relatively small number of HMW glutenin

subunits in any particular wheat variety normally allows resolution of all components [80]. However, complex spectra are obtained for gliadins [80-82] and LMW glutenin subunits [80], consistent with the large number of individual components [69,70] in each protein group.

Bloch et al [82] showed that the majority of gliadin peaks occur in the 27-45 kDa range with another group evident in the 14-20 kDa range. The largest peaks were in the 27-34 kDa range with one or several broad peaks dominating this region. Based primarily upon this region, they demonstrated that artificial neural network classification could be used to identify spectra from 100 samples representing 10 varieties with 97% accuracy.

In our laboratory, we have been able to achieve much improved mass resolution of gliadins (and LMW glutenin subunits) by using delayed extraction of desorbed ions into the TOF mass spectrometer relative to that obtained using constant voltage [80]. Gliadin spectra were obtained showing a large number of well resolved peaks in the 30-40 kDa range, an example of which is shown in Fig. 4.1. These results suggest that direct analysis of gliadin mass spectra might be suitable for variety identification. In the present study, we report on the ability of MALDI-TOF MS to identify sixteen varieties representing four different Canadian wheat classes. Selected varieties grown at a number of locations were also assessed to determine the impact of environment on mass spectral patterns.

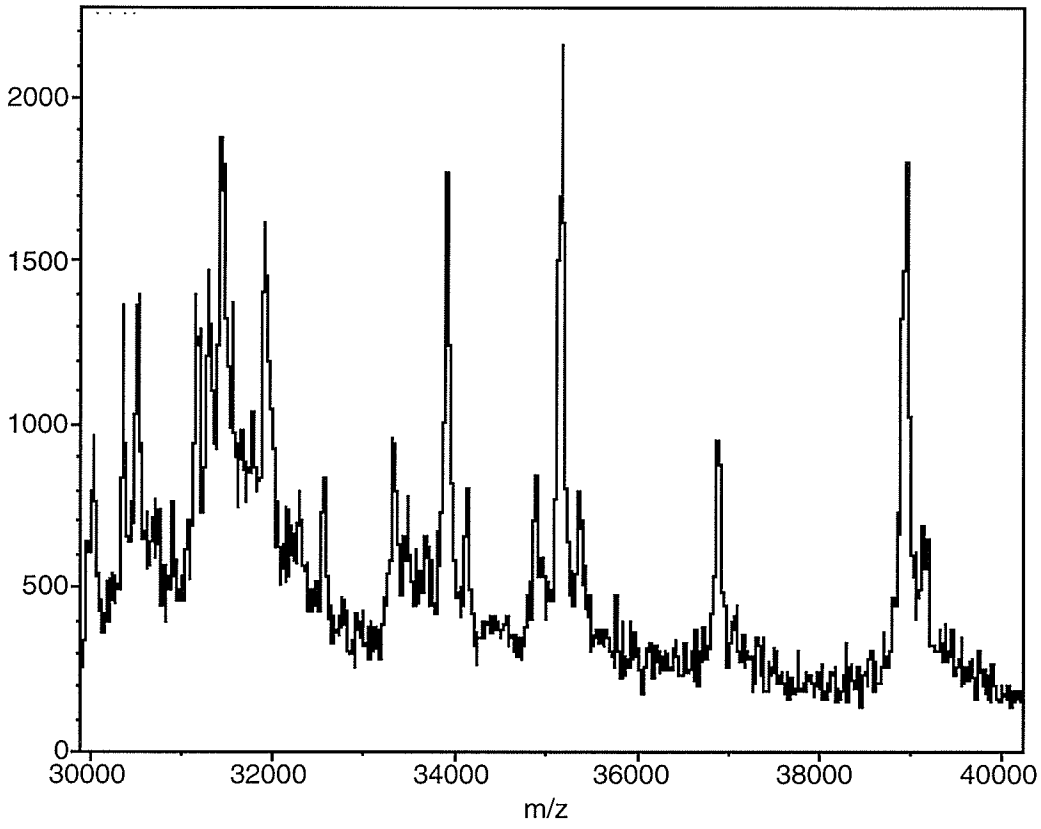

Fig 4.1. Biggar gliadin spectrum over mass range 30k-40k Da

4.2 Materials And Methods

4.2.1 Wheat Samples

Two sets of samples were used. The first set was obtained from a reference collection of pure wheat variety samples maintained at the Grain Research Laboratory for variety identification using our acid PAGE system and included sixteen varieties representing four Canadian wheat classes. Varieties included

Glenlea and Wildcat representing the Canada Western Extra Strong (CWES) wheat class; Arcola, Kyle, Medora, and Waskana representing the Canada Western Amber Durum (CWAD) wheat class; AC Crystal, AC Taber, and Biggar representing the Canada Prairie Spring Red (CPSR) wheat class; AC Vista representing the Canada Prairie Spring White (CPSW) wheat class and CDC Teal, Columbus, Katepawa, Laura, Leader, and Robin representing the most widely grown Canada Western Red Spring (CWRS) wheat class. Wheat samples from high grade sites, as assessed by Canadian Grain Commission inspectors, were also obtained from the 1996 Saskatchewan wheat variety trials to assess the impact of environment. Sites included Rosthern, Wynyard, Battleford, Fox Valley, Kernen, Kelvington, Shellbrook, and Girvin. Varieties tested included Kyle (CWAD), AC Melita (CWAD), Katepwa (CWRS), CDC Teal (CWRS), AC Karma (CPSW) and AC Crystal (CPSR). All samples were subjected to acid PAGE as described by Tkachuk and Mellish [67] to confirm variety purity before further testing.

4.2.2 Extraction and Preparation of Samples For MS

Samples were ground in a grinder equipped with a 1.0 mm screen. Gliadins were extracted from ground grain with 600 µl of 70% ethanol at room temperature for 1 hour in 1.5 mL micro-centrifuge tubes with mixing every 10 min using a vortex mixer. Centrifugation was carried out at 8800 g for 10 min using an Eppendorf microcentrifuge. The supernatant was retained for analysis.

A saturated matrix solution was prepared by dissolving excess sinapinic acid (3,5-dimethoxy-4-hydroxycinnamic acid) in an aqueous 50% acetonitrile solution containing 0.1% of trifluoroacetic acid. The solution was mixed with a vortex stirrer and then centrifuged for 10 seconds to settle the undissolved matrix. A 10:1 matrix to gliadin extract solution was prepared and 3 μL was placed on a metal target probe and dried with a hot air blower to form a deposit about 2 mm in diameter. Approximately 4 samples can be applied to the probe in addition to an external calibrant normally placed at the center. For these measurements, myoglobin (from sheep heart, 16951 Da) was used as the calibrant. The samples were also mixed with myoglobin and run again for more accurate mass determination with an internal calibration

4.2.3 MALDI-TOF MS

Positive ion spectra were obtained on an in-house [83] TOF instrument in the linear mode with delayed extraction as described
previously [80]. A nitrogen laser (VSL 337 ND, Laser Science, Cambridge, MA, USA) was used to illuminate the target with a pulse frequency of 2-3 Hz. A two-grid delayed extraction system [53] was employed using a 25 kV d.c. accelerating potential on the probe and first grid with a pulse of 3 kV applied to the probe 1.2 μs after the laser pulse. After desorption, and acceleration, ions drift through a field-free region of 1.2 m in which the nominal pressure is 3×10^{-7}

Torr. Ions were detected with microchannel plates and the signal was recorded with a transient recorder (LeCroy TR8828D). Spectra were summed by a Macintosh computer.

Approximately 150-200 shots were accumulated per spectrum. Digital files of m/z versus intensity spectra were converted to compact grey-scale or false-colour plots using in house acquisition and analysis software (TOFMA) to facilitate comparison among varieties.

4.2.4 Calibration of Gliadin Spectra

For identifying the gliadin patterns, it is clearly desirable to avoid the interference introduced by mixing the sample with a calibrant. However, calibrant mixtures were used to improve the consistency of the calibration between experiments in the following way. The mass spectra of the mixture of the gliadin sample with the myoglobin calibrant were used (with internal calibration) to identify accurately the mass of one prominent gliadin peak. Where possible, the same peak was used for all the varieties within a class. The mass spectra of the unmixed gliadin samples were first calibrated using the external myoglobin spectrum obtained under identical conditions. Then single-point internal recalibration was performed using the prominent gliadin peak identified from the

mixture. This recalibration changes only the slope in the calibration, using the time offset from the external calibration; the time offset is much less sensitive to variations in voltage, temperature or the position of the sample on the probe. This calibration procedure involves considerable effort but is only necessary here to establish the spectral patterns. In applications of this method to identify an unknown, the separate internal calibration spectrum is not necessary, and the internal re-calibration can be done by matching the mass of a prominent gliadin peak (determined with external calibration), to a table of likely candidates.

4.3 Results And Discussion

The mass range of the gliadin proteins examined was between 30 kDa and 40 kDa where most of the peaks occur [80]. Previous studies have demonstrated that the use of delayed extraction gives substantial improvements in mass resolution in this mass range [80]. This proved to be essential in variety identification because of the large number of peaks which could be identified. In some cases, more than 100 resolved peaks were evident from spectra representing individual hexaploid varieties.

Potential genetic relationships among varieties, which could impact gliadin patterns, were assessed using pedigree information available from the CIMMIT database [84] and from discussions with Canadian wheat breeders (personal communications).

4.3.1 Class And Variety Identification By MALDI-TOF MS

MALDI-TOF MS grey-scale spectra plots (obtained from spectra such as shown in Fig 4.1) of the gliadin extracts from sixteen Canadian wheat varieties representing four Canadian wheat classes (cps, cwad, cwes, cwrs) obtained from the Grain Research Laboratory collection are shown in Figure 4.2. Data range is from 30000 to 40000 Da.

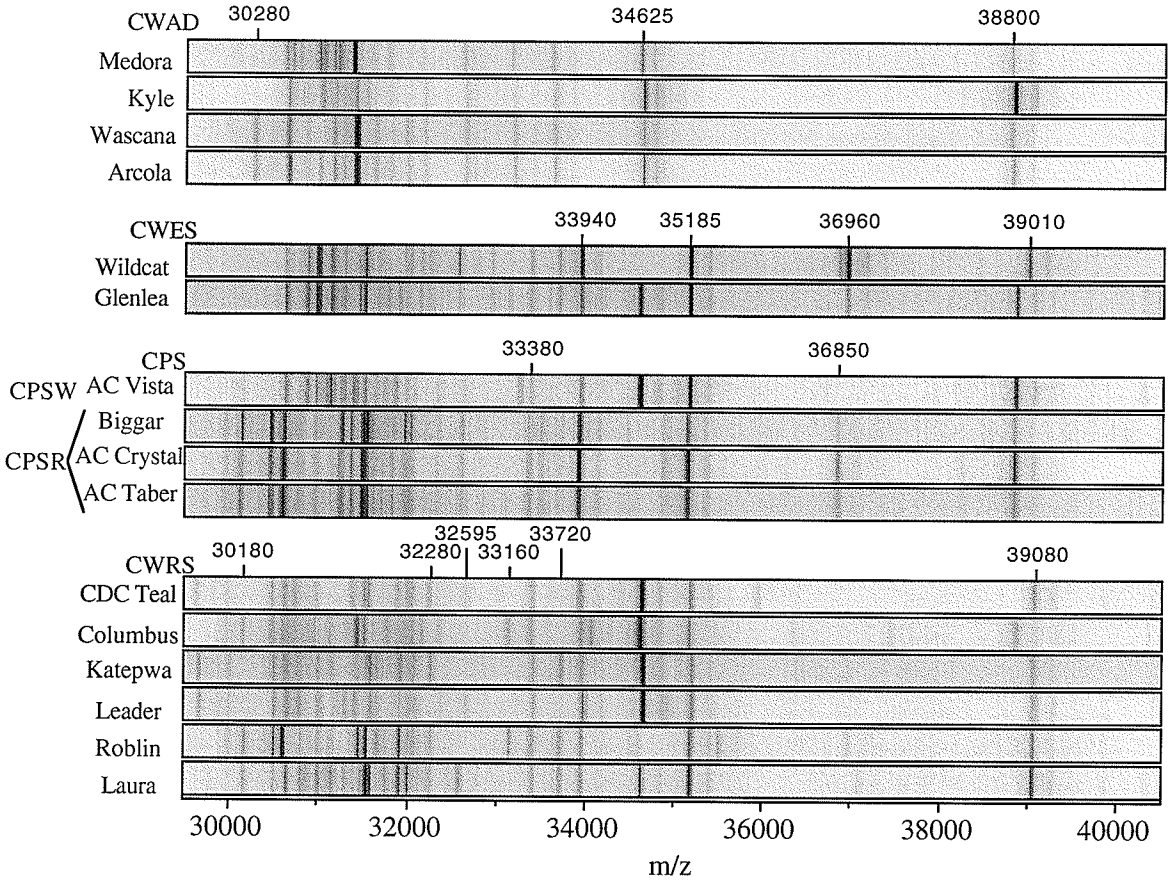

Fig 4.2. Grey-scale plots of gliadin spectra, from 30-40 k*Da

Differences are clearly evident in patterns between wheat classes. In general, varieties within each wheat class showed a number of strong, easily identifiable bands, which were common to the class and were lacking in the other wheat classes. This similarity is probably a reflection of similar genetic backgrounds due to the extensive use of older varieties or parental material thereof in crosses to maintain the characteristic inherent quality characteristics required in each class to allow registration and release of new varieties [85]. In most cases, varieties within each wheat class could also be easily identified by the absence or presence of a few strong or medium intensity peaks. For some varieties, more careful examination of less prominent peaks was required for identification.

Fig. 4.2 shows peaks used in this study to identify the sixteen varieties representing four Canadian wheat classes. Peaks were normally considered to represent the same ion if they were within a range of ±50 Da. In addition, some leeway was given for broader (unresolved) peaks, which presumably consist of more than one protein with very similar m/z value.

Table 4.1 indicates the peaks used to differentiate classes from each other. The most relevant peaks referred to in the following sections are denoted with colours.

Table 4.1 Peak identities used for class distinction. Absence of a peak is represented by a dot when used for identification.

	30180	30280	32280	32595	33160	33380	33720	33940	34625	35185	36850	36960	38800	39010
CWAD				X	X	·	X		X				X	
Medora				X	X	·	X		X				X	
Kyle				X	X	·	X		X				X	
Wascana		X		X	X	·	X		X				X	
Arcola		X		X	X	·	X		X				X	
CWES			X	X		X	X	X		X		X		
Wildcat			X	X		X	X	X		X		X		
Glenlea			X	X	X	X	X	X	X	X		X	X	
CPS				X		X		X		X				
AC Vista				X		X		X	X	X			X	
Biggar	X	X		X		X		X		X	X		X	
AC Crystal	X	X		X		X		X		X	X		X	
AC Taber	X	X		X		X		X		X	X		X	
CWRS						X		X		X				
CDC Teal			X	X		X		X	X	X				X
Columbus	X				X	X		X	X	X			X	
Katepwa			X			X	X	X	X	X				X
Leader				X		X		X	X	X				X
Roblin	X		X		X	X	X	X		X				X
Laura	X		X	X		X	X	X	X	X				X

CWAD VARIETIES

For CWAD wheat, peaks at 33160 and 34625 Da were common to all four varieties but were not common in all varieties from any other wheat class. Other varieties that did have a peak at 33160 also had a peak at 33380, which was not present in the CWAD varieties.

Differences in the four CWAD varieties, as shown in Fig. 4.3, were most evident among the peak profiles in the 30k-32k Da range. Arcola and Wascana showed a peak at 30280 Da absent in the other varieties while Medora showed a much more intense peak at 30720 Da relative to the other cultivars. Arcola, which was derived from a Wascana cross, has a peak at 31015 Da not present in Wascana. And Kyle could be distinguished from the other CWAD varieties from its peak at 31550.

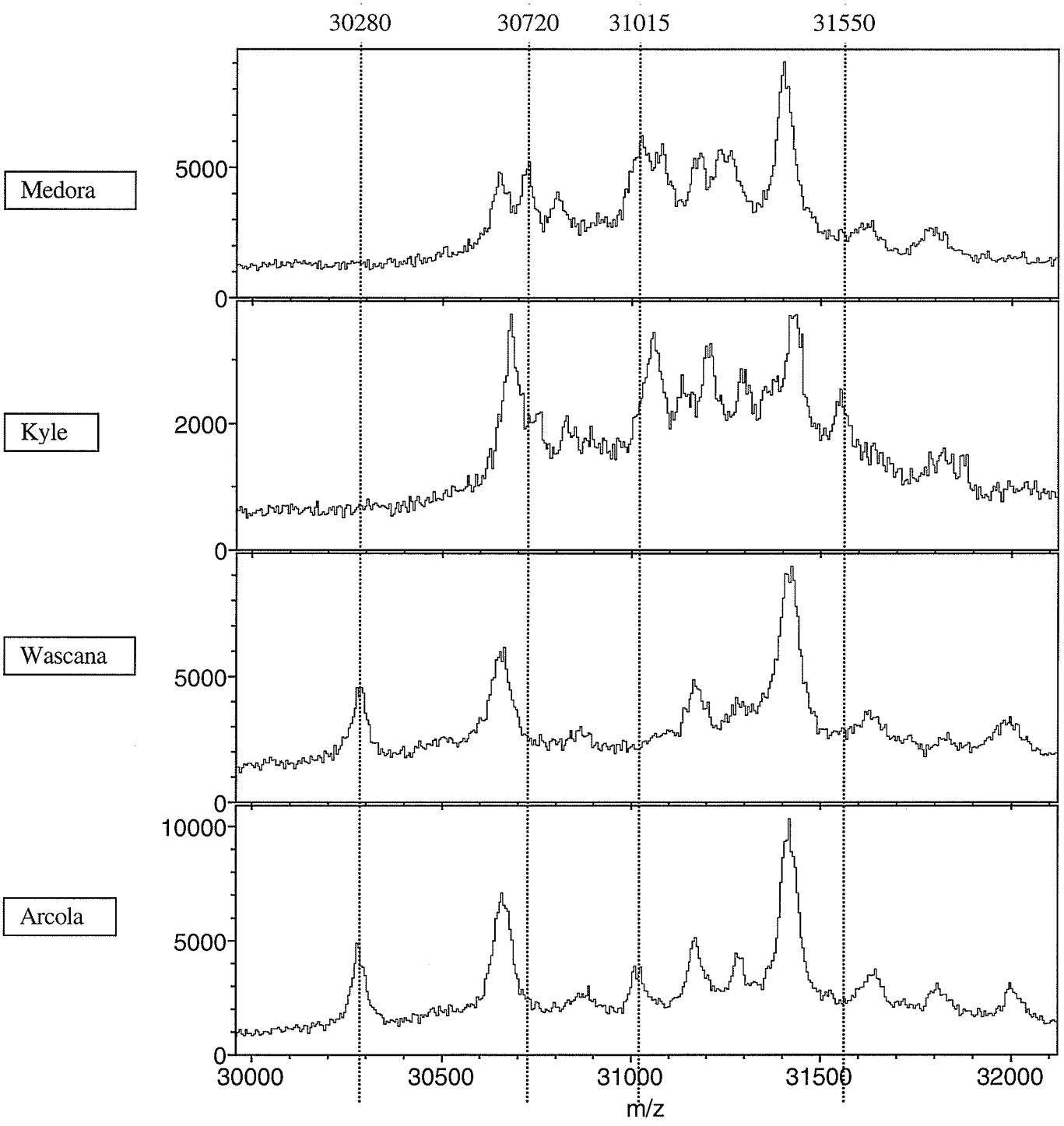

Fig 4.3 CWAD varieties

CWES VARIETIES

Differences in the expression of a few predominant peaks were sufficient to differentiate among varieties within the CWES and other wheat classes. In the CWES class there is a peak at 36960 absent in any other class. As shown in Fig. 4.2, a number of additional peaks present in only one of the two CWES cultivars (33160 and 34625 in Glenlea) identify the two CWES varieties from each other.

CPS VARIETIES

All CPSR and CPSW varieties showed characteristic strong peaks at 33380 and 38800 Da, which occurred only in two varieties (Columbus and Glenlea) outside the CPS class. Columbus and Glenlea had a peak at 33160, which distinguished it from the CPS varieties. Although AC Vista could be identified from the three CPSR varieties (Biggar, AC Crystal, and AC Taber) with its peak at 34625, the three CPSR varieties did not have sufficient differences to be differentiated. The 34625 Da peak in AC Vista is probably inherited from the top cross parent, HY 358, which is derived from the CWES cultivar, Glenlea [85].

CWRS VARIETIES

CWRS wheat varieties have been developed using extensive backcrossing to the same or closely related parents (Marquis type) to maintain the uniform high inherent quality in the class [86]. However, differences in patterns among the six CWRS cultivars were still clearly evident in spite of the similar genetic background (Figure 4.2). All six CWRS wheat varieties showed

strong peaks (within error) at 33380, 33940 and 35185 Da while five of the six varieties showed a strong peak at 39073 Da. (These peaks were used as internal calibrants for examination of the spectra with these peaks in common.) CDC Teal and Leader and Laura showed peaks at 32595 Da absent in the other varieties. Distinguishing these three, Leader lacked the peak present in CDC Teal and Laura at 32280 Da and Laura had a peak at 33720 absent in CDC Teal and Leader. Columbus showed a distinctive peak at 38800 absent from other CWRS varieties, while Roblin had a peak at 33160 not present in Katapwa and lacked the prominent peak at 34625 Da evident in all other varieties. Laura and Katepwa showed very similar spectra but could be identified by the peaks at 30180 and 33160 present in Laura but not Katepwa.

4.3.2 Effects Of Environment

To determine the effects of environment on MALDI-TOF MS spectra of gliadin mixtures selected CWRS, CWAD, CPSR and CPSW varieties grown at six sites in the 1996 Saskatchewan wheat trials were examined. Examples of spectra of these samples are shown in Fig.4.4, Fig 4.5, and Fig 4.6, with the location shown in brackets.

AC Karma

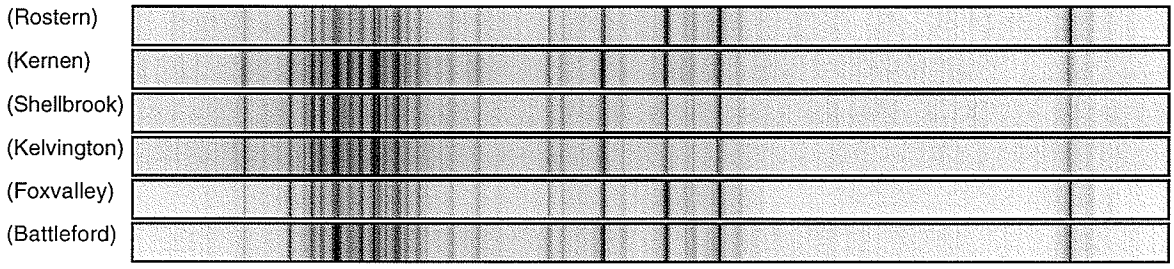

AC Crystal

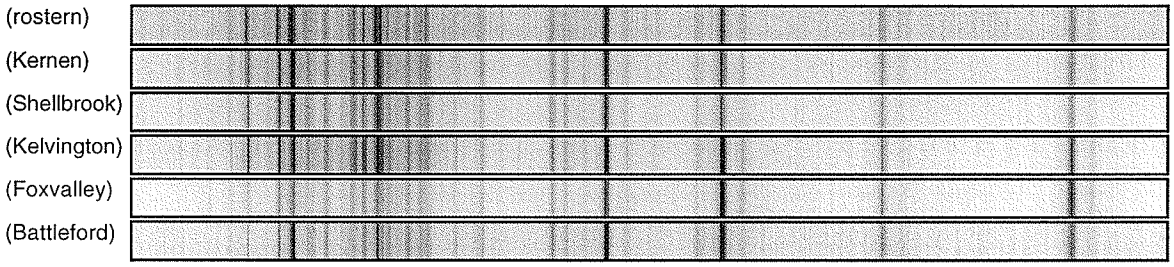

Fig.4.4 CPS varieties in different environments

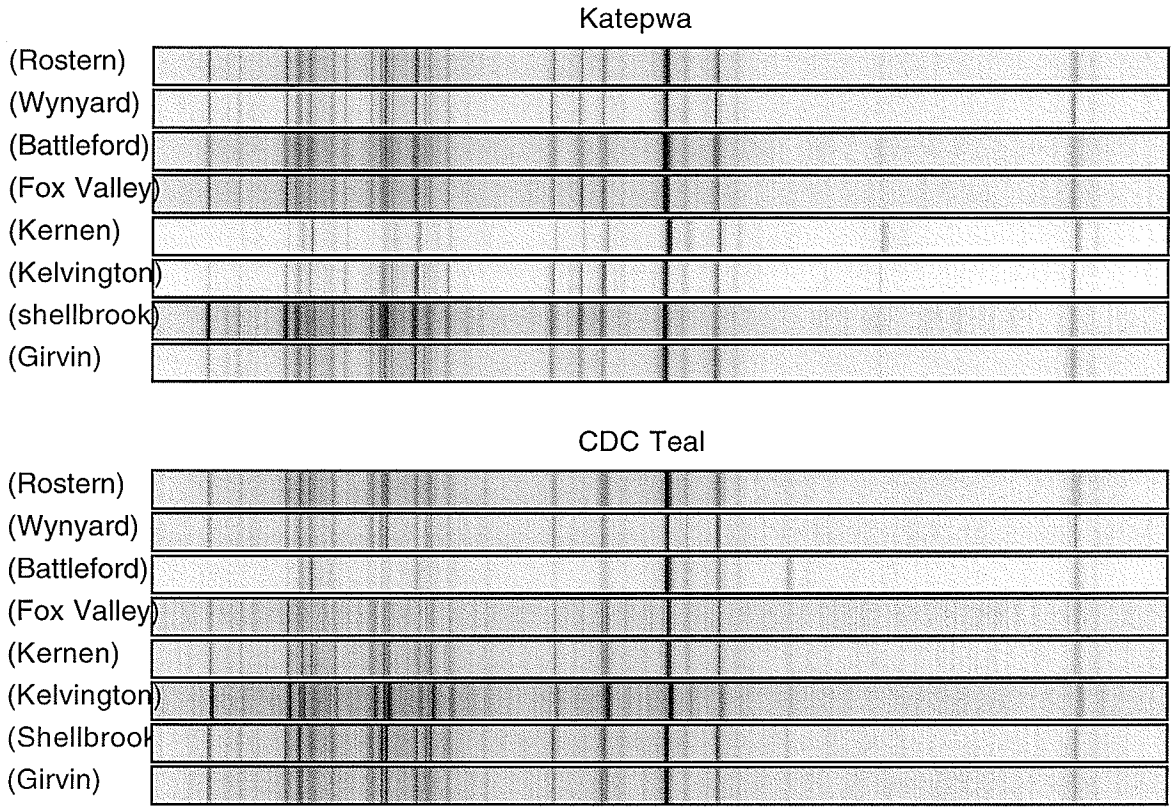

Fig 4.5 CWRS varieties in different environments

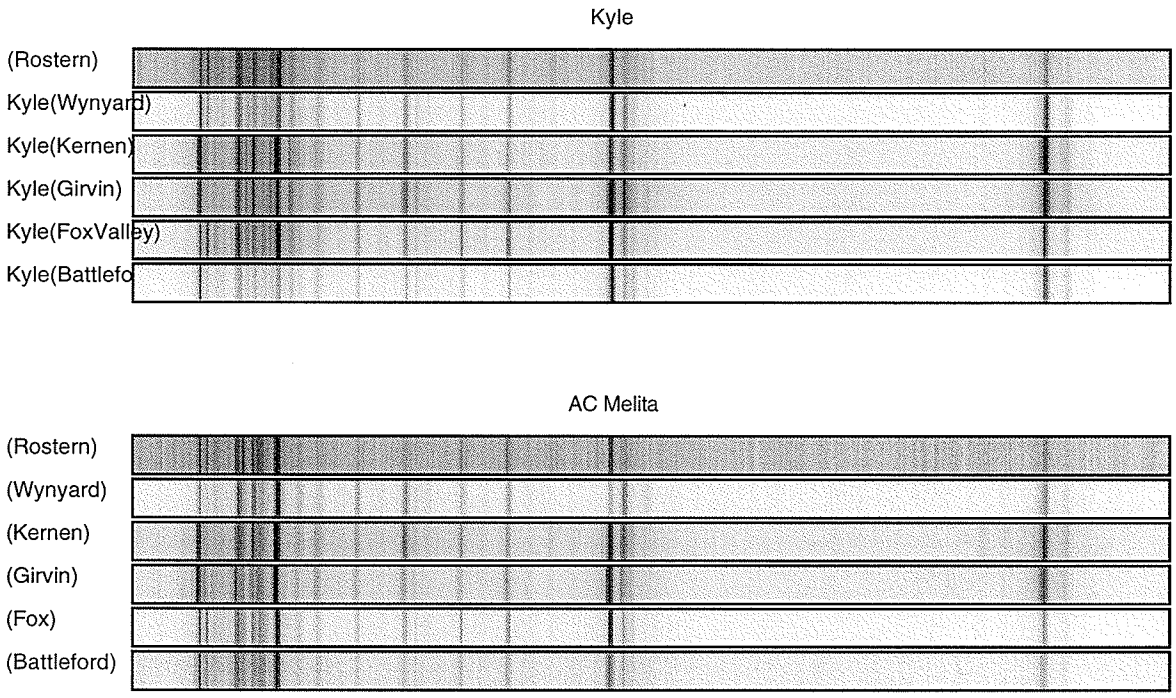

Fig 4.6 CWAD varieties in different environments

Little change was evident in patterns obtained for two CWAD wheat varieties (Kyle, AC Melita), one CPSR wheat variety (AC Crystal) and one CPSW wheat variety (AC Karma). The CWRS varieties, Katepwa and CDC Teal, showed little change at five of six stations (three stations shown for Katepwa in Fig 4.7). However, in Fig 4.5 some peaks seemed to be faint or absent for CDC Teal grown at Battleford (Fig 4.8) and for Katepwa grown at Kernen (Figure 4.9). These differences were most evident at the lower mass range (30k-31k Da). The reasons for this are not known. The decrease in intensity or loss of peaks in this

region did not impede the ability to identify varieties since patterns above this range were not affected and sufficient for this purpose. Overall, these results suggest that environment does not generally have a major impact on MS spectra, consistent with results obtained on the impact of environment on gliadin electrophoretic and HPLC profiles [66,87]

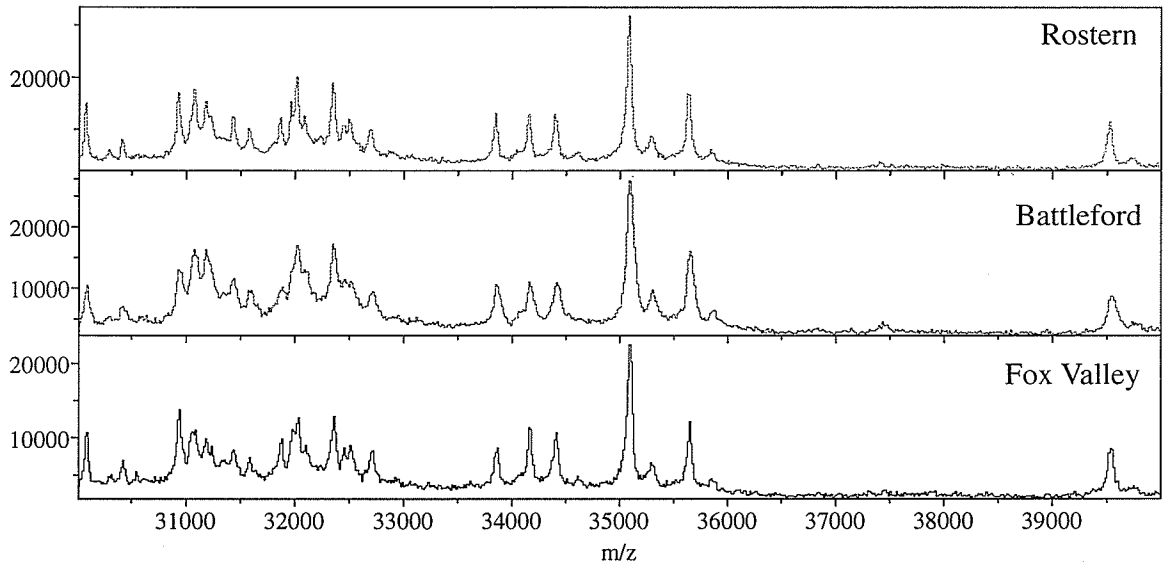

Fig. 4.7 Gliadin spectra for AC Katepwa grown in different environments

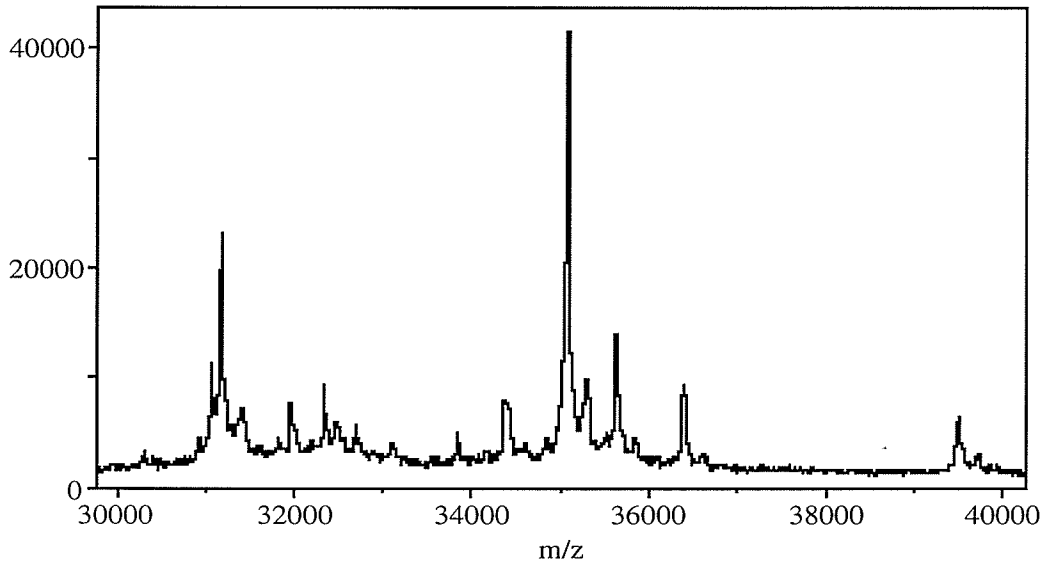

Fig 4.8 CDC Teal grown at Battleford

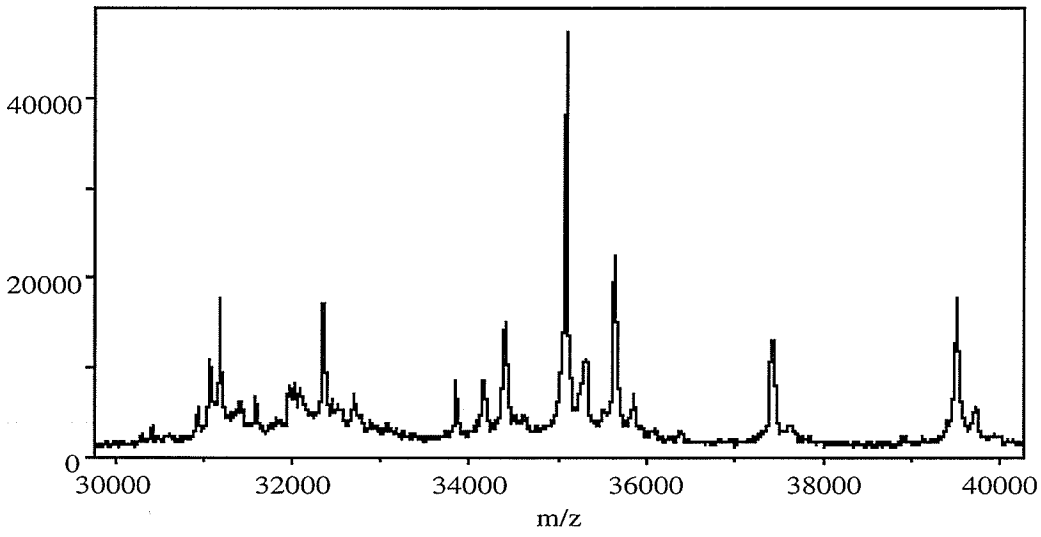

Fig 4.9 Katepwa grown at Kernen

4.4 Conclusions

This study has demonstrated the ability of MALDI-TOF MS to differentiate among Canadian wheat classes as well as a number of varieties within each class using gliadin protein extracts. Varieties within each of the five wheat classes showed characteristic prominent peaks representative of that class. In most cases, varieties within a class could be easily differentiated based upon the analysis of the presence or absence of medium to strongly expressed peaks while, for a few very closely related varieties, more careful examination of less prominent peaks was required for identification. Overall, these results suggest that MALDI-TOF MS shows promise as an alternative method to procedures involving acid PAGE [55-58], RP-HPLC [7] and capillary electrophoresis [72-73] for wheat class and variety identification.

A major constraint to the use of MALDI-TOF MS for wheat variety identification is the current high cost of the instrumentation. With rapid advancements occurring in instrumentation, costs may be reduced in the near future to levels similar to RP-HPLC and capillary electrophoresis but would still be significantly higher than the cost of acid PAGE equipment, the most widely used method. However, there may be several advantages related to this technique relative to acid PAGE for variety identification including the ability to automate and thus increase throughput, higher resolution as evidenced by

spectra showing upwards of 100 peaks which could potentially allow greater differentiation of very closely genetically related varieties and faster analysis (< 2 min/sample after extraction and about 20 sec/sample after drying the matrix and sample on metal probes). Recent studies [88] have shown that multiple gliadin extracts can also be absorbed with matrix onto polyurethane membranes and then analyzed directly from the membranes at a later time, allowing sample preparation to occur off-site. Quantification of MS peaks may also be possible as shown by Nelson and co-workers [89] for a range of animal proteins. This approach suggests potential for quantification of classes/varieties present in commercial samples involving mixtures, which currently require single kernel analysis.

The high resolution of MALDI - TOF MS also suggests applications in the study of the genetic control of wheat proteins, which are closely related to quality [90]. In particular, the ability to accurately measure protein masses and the extremely high sensitivity (< 1 picomole) of the technique may be very useful when combined with PAGE, RP-HPLC or capillary electrophoresis for generation of two dimensional wheat protein plots. Studies have shown that PAGE bands can be blotted or excised [91] while peaks from HPLC [79] or capillary electrophoresis [92] can be easily transferred to target probes or membranes for MALDI-TOF MS.

REFERENCES

[1] J.J. Thomson, *Philos. Mag.* VI, **24,**209,668 (1912).

[2] A.J. Dempster, *Phys.Rev.***11**,316 (1918).

[3] F.W. Aston, *Philos. Mag.* **38**, 709 (1919).

[4] F.A. White and G.M. Wood, *Mass Spectrometry, Applications in Science and Engineering,* John Wiley & Sons, Chichester, England, (1986).

[5] D.F. Torgerson, R.P. Skowronski and R.D. Macfarlane, *Biochem, Biophys. Res. Commun.* **60**, 616 (1974)

[6] R.D. Macfarlane and D.F. Torgerson, *Science* **191** (1976) 920

[7] B.U.R. Sundqvist, P. Roepstorff, J. Fohlman, A. Hedin, P. Håkansson, I. Kamensky, M. Lindberg, M. Salephour and G. Säve, *Science* **226** (1984) 696

[8] G. Jonsson, A. Hedin, P. Hakansson and B.U.R. Sundqvist, *Rapid Commun. Mass Spectrom.* **3** (1989) 190

[9] W.E. Stephens, *Phys. Rev.* **69** (1946) 691

[10] A. Benninghoven, D. Jaspers and W. Sichtermann, *Appl. Phys.* **11** (1976) 35

[11] B.T. Chait and K.G. Standing, *Int. J. Mass Spectrom. Ion Phys.* **40** (1981) 185

[12] W. Ens, K.G. Standing, B.T. Chait, and F.H. Field, *Anal. Chem.* **53** (1981) 1241

[13] W. Ens, P. Hakansson, B.U.R. Sundqvist, *Secondary Ion Mass Spectrometry SIMS VI*, Ed. A.M. Buber, A Benninghoven, H.W. Werner and G. Soldzian (Wiley, Chichester

1988) 623; and unpublished data from the same experiment

[14] M. Barber, R.S. Bordoli, G.J. Elliot, R.D. Sedgwick and A.N. Tyler, *Anal. Chem.* **54** (1982) 645A

[15] D.J. Surman and J.C. Vickerman, *J. Chem. Soc. Chem. Commun.* 1981 (1981) 342

[16] M. Barber, R.S. Bordoli, R.D. Sedgwick and A.N. Tyler, *J. Chem. Soc. Chem. Commun.* 1981 (1981) 325

[17] M. Barber, R.S. Bordoli, G.J. Elliot, R.D. Sedgwick, A.N. Tyler and B.N. Green *J. Chem. Soc. Chem. Commun.* 1982 (1982) 936

[18] A. Dell and H.R. Morris, *Biochem. Biophys. Res Commun.* **106** (1982) 1456

[19] E. Unsold, F. Hillenkamp and R. Nitsche, *Analusis* **4** (1976) 115

[20] R.J. Conzemius and J.M. Capellen, *Int. J. Mass Spectrom. Ion Phys.* **34** (1980) 197

[21] F. Hillenkamp, in *Ion Formation from Organic Solids*, IFOS, Ed. by A. Bennighoven, Springer Series in Chem. Phys., **25** (1983) 190–205

[22] F. Hillenkamp, in *Secondary Ion Mass Spectrometry, SIMS V*, Ed. by A. Bennighoven, R.J. Colton, D.S. Simmons and H.W. Werner, Springer Series in Chem. Phys. **44** (1986) 471

[23] F. Hillenkamp, M. Karas, R.C. Beavis and B.T. Chait, *Anal. Chem.* **63** (1991) 1193A

[24] M. Karas, B. Bachmann, U. Bahr and F. Hillenkamp, Int. J. Mass Spectrom. Ion Processes 78 (1987) 53

[25] M. Karas and F. Hillenkamp, *Anal. Chem.* **60** (1988) 2299

[26] R.C. Beavis and B.T. Chait, *Rapid Commun. Mass Spectrom.* **3** (1989) 233

[27] R.C. Beavis and B.T. Chait, *Rapid Commun. Mass Spectrom.* **3** (1989) 432

[28] A. Overberg, M. Karas and F. Hillenkamp, *Rapid Commun. Mass Spectrom.* **5** (1991)

[29] W.E. Stephens. *Phys. Rev.* **69**, (1946) 691

[30] A.E. Cameron and D.F. Eggers, Jr., *Rev. Sci. Instrum.* **19**, (1948) 605

[31] Mamyrin BA, Karataev VI, Shmikk DV and Zagulin VA (1973) The mass-reflectron, a new nonmagnetic time-of-flight mass spectrometer with high resolution. *Soviet Physics - JETP* **37:** 45-48.

[32] P. Juhasz,M. Vestal,S. A. Martin, Proceedings of the 44th ASMS conference on Mass Spectrometry and Allied Topics, Portland, May 12-16, 1996, p.730.

[33] M. Schurencerg, T. Schulz, K. Dreisewerd, F. Hillenkamp, Rapid Commun. Mass Spectrom., 10(1996) 1873.

[34] Gluckmann-M., Karas-M, Journal of mass spectrometry, Vol 34, pp 467-477, (1999)

[35] R.C. Beavis, B.T. Chait, Chem. Phys. Lett., 181(1991) 479.

[36] Zhang-W.Z.,Chait-B.T.,Int. Journal of mass spectrometry and ion processes,160(1997) 259

[37] Y.Pan, R.J. Cotter, Org. Mass Spectrom., 27 (1992) 3.

[38] A.Verentchikov, W. Ens, J. Martens, K.G. Standing, Proceedings of the 40th ASMS Conference on Mass Spectrometry and Allied Topics, Washington, May 31-June 5, 1992, p. 361

[39] G. Kinsel, D.H. Russel, Proceedings of the 40th ASMS Conference on Mass Spectrometry and Allied Topics, Washington, May 31- June 5 , 1992, p. 1928.

[40] R.G. Dworschak, V. Spicer, W. Ens, K.G. Standing, Proceedings of the 46th ASMS Conference on Mass Spectrometry and Allied Topics, Orlando, May 31- June 4, 1998 p. 932.

[41] T. Huth-Fehre, C.H. Becker, Rapid Commun, Mass Spectrom., 5 (1991) 378.

[42] J. Zhou, W. Ens, K.G. Standing, A. Verentchikov, Rapid Commun. Mass Spectrom., 6 (1992) 671.

[43] B. Spengler, V. Bokelmann, Nucl. Instrum. Meth. Phys. Res. B, 82 (1993) 379.

[44] V. Bokelmann, B. Spengler, R. Kaufmann, Eur. Mass Spectrom., 1 (1995) 81.

[45] W.Z. Zhang, B.T. Chait, Int. J. Mass Spectrom. Ion Processes, 160 (1997) 259.

[46] G.R. Kinsel, R.D. Edmondson, D.H. Russel, J. Mass Spectrom., 32 (1997) 714.

[47] A.A. Puretzky, D.B. Geohegan, G.B. Hurst, Phys. Rev. Lett., 83 (1999) 444.

[48] G.R. Kinsel, M.E. Gimon-Kinsel, K.J. Gillig, D.H. Russel, J. Mass Spectrom.,34 (1999) 684.

[49] B. Spengler, U Bahr, M. Karas and F. Hillenkamp, Anal. Instrum. 17 (1988) 173.

[50] B. Spengler, U. Bahr and F. Hillenkamp, in: Resonance Ionization Spectroscopy (1988), eds.

[51] T.B. Lucatorto and J.E. Parks, The Institute of Physics Conf. Ser. 94 (1988) p. 137.

[52]. Brown, R. S. and Lennon, J. Anal. Chem. 67(1995) 1998.

[53] P. Juhasz, M. L. Vestal, S.A. Martin, *J Am Soc Mass Spectrometry* **8** (1997) 209-217

[54] M. Gluckmann, M. Karas, *J . Mass Spectrom.* **34,** (1999) 467-477

[55] RE. Johnson ,Y. LeBeyec, *Int J Mass Spectrom* **177 (2-3)** (1998) 111-118

[56] S. Berkenkamp, C. Menzel, F. Hillenkamp, K. Dreisewerd, J Am Soc Mass Spectrom **13** (2002) 2009-220

[57] X. Tang. A Reflecting Time-of-Flight Mass Spectrometer *Ph.D. Thesis University of Manitoba*, (1991) pp 64

[58] J. Grosser, H. Schulz, *J. Phys. D Appl. Phys.* **22**, (1989) 723-729

[59] K.F. Finney, *Cereal Foods World* **30**, (1985)794

[60] F. MacRitchie, *J. Cereal Sci.* **6**, (1987) 259

[61] R.A. Orth and W. Bushuk, *Cereal Chem.* **49**, (1972) 268

[62] P.I. Payne, *Annu. Rev. Plant Physiol.* **38**, (1987) 141

[63] J.S. Wall, *Recent Advances in the Biochemistry of Cereals,* (1979) Academic Press, London p. 275.

[64] P.R. Shewry and A.S. Tatham, *Biochem.J.* **267**, (1990) 1

[65] 63Du Cros, D. L and Wrigley, C. W. Improved electrophoretic methods for identifying cereal varieties. *J. Sci. Food Agric.* **30** (1979) 785-794.

[66] Zillman, R. R. and Bushuk, W. Wheat cultivar identification by gliadin electrophoregrams. II. Effects of environmental and experimental factors on the gliadin electrophoregram. *Can. J. Plant Sci.* **59** (1979) 281-286.

[67] Tkachuk, R. and Mellish, J. Wheat cultivar identification by high voltage gel electrophoresis. *Ann. Technol., agric.* **29** (1980) 207-212.

[68] Lookhart, G. L. and Finney, K. F. Polyacrylamide gel electrophoresis of wheat gliadins: The effect of environment and germination. *Cereal Chem.* **61** (1984) 496-499.

[69] Bietz, J. A. And Simpson, D. G. Electrophoresis and chromotography of wheat gliadin: Available methods and procedures for statistical.

[70] Bean, S. R. and Lookhart, G. L. Separation of wheat proteins by two-dimensional reversed-phase high -performance liquid chromatography plus free zone capillary electrophoresis. *Cereal Chem.* **74** (1997) 758-765.

[71] Burnouf, T. and Bietz, J. A. Identification of wheat cultivars and prediction of quality by reversed-phase high-performance liquid chromatographic analysis on endosperm

storage proteins. *Seed Sci. & Technol.* **15** (1987) 79-99.

[72]. Werner, W. E., Wiktorowicz, J. E. and Kasarda, D. D. Wheat variety identification by capillary electrophoresis of gliadins and high molecular weight glutenin subunits. *Cereal Chem.* **71** (1994) 397-402.

[73]. Lookhart, G. and Bean, S. A fast method for wheat cultivar differentiation using capillary zone electrophoresis. *Cereal Chem.* **72** (1995) 42-47.

[74]. Karas, M., Bahr, U. and Hillenkamp, F. UV laser matrix desorption/ionization mass spectrometry of proteins in the 100,000 dalton range. *Int. J. Mass Spectrom. Ion Processes* **92** (1989) 231-245.

[75]. Beavis, R. C. and Chait, B. T. Rapid, sensitive analysis of protein mixtures by mass spectrometry. *Proc. Natl. Acad. Sci. USA* **87** (1990) 6873-6877.

[76]. Hillenkamp, F., Karas, M., Beavis, R. C. and Chait, B. T. Matrix-assisted laser desorption/ionization mass spectrometry of biopolymers. *Anal. Chem.* **63** (1991) 1193A-1202A.

[77]. Nguyen, D. N. Becker, G. W. and Riggan, R. M. Protein mass spectrometry: *application to analytical biochemistry. J. Chromatogr. A* **705** (1995) 21 21-45.

[78]. Turner, J. B., Gordon, D. B., Garner, G. V., Lord, G. A. and Smith, C. A. Purification of a-gliadins to apparent homogeneity. *Biochem. Soc. Trans.* **22** (1994) 403S.

[79]. Hickman, D. R., Roepstorff, P., Shewry, P. R and Tatham, A. S. Molecular weights of high molecular weight subunits of glutenin determined by mass spectrometry. *J. Cereal Sci.* **22** (1995) 99-103.

[80]. Dworschak, R. G., Ens, W., Standing, K. G., Preston, K. R., Marchylo, B. A., Nightingale, M. J., Stevenson, S. G. and Hatcher, D. W. Analysis of wheat gluten proteins by

matrix-assisted laser desorption/ionization mass spectrometry. *J. Mass Spectrom.* **33** (1998) 429-435.

[81]. Mendez, E., Camafeita, E., San Sebastian, J., Solis, J., Mayer-Posner, F. J., Suckau, D., Marfisi, C and Soriano, F. Direct identification of wheat gliadins and related cereal prolamines by matrix-assisted laser desorption/ionization time -of-flight mass spectrometry. J. Mass Spectrom., *Rapid Commun. in Mass Spectrom.* **30** (1995) S123-S128.

[82]. Bloch, H. A., Kesmir, C., Peterson, M., Jacobsen, S and Sondergaard, I. Identification of wheat varieties using matrix-assisted laser desorption/ionization time -of-flight mass spectrometry and an artificial neutral network. *Rapid Commun. Mass Spectrom.* **13** (1999) 1535-1539.

[83]. Tang, X., Beavis, R. C., Ens, W., Lafortune, F., Schueler, B. and Standing, K. G. . Int. *J. Mass Spectrom.. Ion Processes* **85**(1988) 43.

[84]. Fox, P, N., Magana, R.I., Lopez, C., Sanchez, H., Herrera, R., Vicarte, V., White, J.W., Skovmand, B. and Mackay, M.C. International Wheat Information System. Version 2. Mexico, D.F. CIMMYT (1997)

[85]. DePauw, R. M., McCaig, T. N., Knox, R. E.. Clarke, J. M. Fernandez, M. R. and McLeod, J. G. AC Vista hard white spring wheat. *Can. J. Plant Sci.* **78**(1998) 617-620.

[86]. Preston, K, R., Morgan, B. C. and Tipples, K. H. A review and analysis of export cargo quality data for Canada Western Red Spring wheat: 1973-1986. *Can. Inst. Food Sci. Technol. J.* **5**(1988) 520-530.

[87]. Huebner, F. R. and Bietz, J. A. Quantitative variation among gliadins of wheats grown in different environments. *Cereal Chem.* **65**(1988) 362-366.

[88]. M. E. McComb, M. E. Oleschuk, R. D. Chow, A. Perreault, H. Dworschak, R. G. Znamirowski, M. Ens, W. Standing K. G.and Preston K. R. Application of non-porous polyurethane thin films and porous PU membranes as sample supports for MALDI MS of wheat proteins J. Mass Spectrometry in press.

[89]. Nelson, R. W., McLean, M. A. and Hutchens, T. W. Quantitative determination of proteins by matrix-assisted laser desorption/ionization time-of-flight mass spectrometry. *Anal. Chem.* **66** (1994) 1408-1415.

[90]. Payne, P. Genetics of wheat storage proteins and the effect of allelic variation on bread-making quality. *Ann. Rev. Plant Physiol.* **38** (1987) 141-153.

[91]. Patterson, S. D. From electrophoretically separated protein to identification: Strategies for sequence and mass analysis. *Anal. Biochem.* **221**(1994) 1-15.

[92]. Weinmann, W., Parker, C. E., Deterding, L. J., Papac, D. I., Hoyes, J., Przybylski, M and Tomer, K. B. Capillary electrophoresis - matrix-assisted laser-desorption ionization mass spectrometry of proteins. *J. Chrom.* A. **680** (1994) 353-361.

[93] Copyright (c) 1981-1988 by Waterloo Maple Inc.

[94] Gluckmann, M., Karas, M. *J. mass spectrom* **34** (1999), 467-477.

[95] R.G. Dworschak, Proceedings of the 47th ASMS conference on Mass Spectrometry and Allied Topics, Dallas, TX, June 13-17. , Ph.D. Thesis, University of Manitoba.

Appendix A

For a more exact analysis of the time of flight with delayed extraction, the time spent during acceleration must be considered. These can be calculated from Newton's 2nd law:

$$t_1 + t_2 = \frac{m(v_1 - v_0)}{qE_1} + \frac{m(v_2 - v_1)}{qE_2}$$

where v1 and v2 are the velocities at the first and second grids, E1 and E2 are the electric fields in the two regions, and m and q are the mass and charge of the ions. The velocities can be determined from the respective kinetic energies:

$$T_0 = \frac{1}{2}mv_0^2$$

$$T_1 = T_0 + qV_p\left(1 - v_0\frac{\tau}{d_1}\right) = \frac{1}{2}mv_1^2$$

$$T_2 = T_1 + qV_2 = \frac{1}{2}mv_2^2$$

and the electric fields are simply

$$E_1 = \frac{V_p}{d_1}, E_2 = \frac{V_2}{d_2}$$

With these substitutions, the time-of-flight can be expressed as a function of the initial velocity, the delay time τ, applied voltages, and geometrical constants. Calculated time-of-flights as a function of tau for typical values of the constants and for initial velocities up to1000 m/s show an almost perfect linear dependence. Indeed, a first order series expansion of the function about the ratio of the initial velocity to the nominal velocity v_0 of an accelerated ion (*1/2 mv^2 = q* V_a) is linear in tau:

$$t = \frac{L_e}{v} + (\alpha\tau + \beta)\frac{v_0}{v}$$

with the slope proportional to α:

$$\frac{dt}{d\tau} = \alpha\frac{v_0}{v}$$

The nominal velocity can be determined from the nominal time from

$$v = \frac{L_e}{t}$$

so that the initial velocity can be determined from the slope and nominal time:

$$v_0 = \frac{dt}{d\tau} L_e \frac{\alpha}{t}$$

The constants L_e and α can be extracted from the explicit series expansion and following Juhasz [53], can be expressed using only the ratio of the grid voltage to the total accelerating voltage

$$G = V_g(V_p + V_g)$$

and geometrical constants:

$$L_e\alpha = \left(L + 2\frac{d_2}{\left(1+(1-G)^{\frac{1}{2}}\right)} + 2\frac{d_1}{(1-G)^{\frac{1}{2}}} \right) 2\frac{d_1}{(1-G)L + 2(1-G)^{\frac{1}{2}}\frac{d_2}{\left(1+(1-G)^{\frac{1}{2}}\right)} - 2\frac{d_1}{(1-G)^{\frac{1}{2}}}}$$

Appendix B

The time of flight equations, given below, for ions that are subject to delayed extraction and reflected by a mirror were graphed in the math program Maple. This was used to model what the expected results of a time of flight vs delay curve should look like under typical acceleration and pulse voltages, as well as reasonable values of initial velocity for the ions. E1,E2 and E3 refer to the electric fields in the target and first grid, the first grid and grounding grid, and the mirror respectively. T0,T1, and T2 are the kinetic energy values of the ion initially, after the delayed extraction region, and in free flight respectively. z is the charge of the ion. v0 is the initial velocity of the ion. m is the mass of the ion. The delay time is given by the variable D. U is the target plus pulse voltage, while G is the ratio of target voltage over pulse and target combined. The equation at the end of this appendix gives the time of flight with the initial velocity as the only unknown variable.

```
> T1:= z*(1-G)*U +1/2*m*v0^2 - v0*D*z*E1;
```

```
> T2:= z*U +1/2*m*v0^2 - v0*D*z*E1;
```

```
> G:=volt/U;

> U:=pulse+volt;

> T0:=(m*v0^2)/2;

> E1:=(1-G)*U/d1;

E1 := (1-volt/(pulse+volt))*(pulse+volt)/d1

> E2:=G*U/d2;

E2 := volt/d2

> E3:= 4*U/(L);

E3 := 4*(pulse+volt)/L

> t:=(sqrt(2*m)/z)*((sqrt(T1)-sqrt(T0))/E1+(sqrt(T2)-sqrt(T1))/E2);
```

t := sqrt(2)*sqrt(m)*((1/2*sqrt(4*z*(1-volt/(pulse+volt))*(pulse+volt)+2*m*v0^2-
4*v0*D*z*(1-volt/(pulse+volt))*(pulse+volt)/d1)-1/2*sqrt(2)*sqrt(m*v0^2))*d1/((1-
volt/(pulse+volt))*(pulse+volt))+(1/2*sqrt(4*z*(pulse+volt)+2*m*v0^2-4*v0*D*z*(1-
volt/(pulse+volt))*(pulse+volt)/d1)-1/2*sqrt(4*z*(1-
volt/(pulse+volt))*(pulse+volt)+2*m*v0^2-4*v0*D*z*(1-
volt/(pulse+volt))*(pulse+volt)/d1))*d2/volt)/z

> t3:=L*sqrt(m/(2*T2));

t3 := 1/2*L*sqrt(2)*sqrt(m/(z*(pulse+volt)+1/2*m*v0^2-v0*D*z*(1-
volt/(pulse+volt))*(pulse+volt)/d1))

> t4:=d3*sqrt(m/(2*T1));

t4 := 1/2*d3*sqrt(2)*sqrt(m/(z*(1-volt/(pulse+volt))*(pulse+volt)+1/2*m*v0^2-
v0*D*z*(1-volt/(pulse+volt))*(pulse+volt)/d1))

> t5:= 2*sqrt(2*m*T2)/(z*E3);

t5 := 1/2*sqrt(2)*sqrt(m*(z*(pulse+volt)+1/2*m*v0^2-v0*D*z*(1-
volt/(pulse+volt))*(pulse+volt)/d1))*L/(z*(pulse+volt))

```
> tof:=t+t3+t4+t5;

tof := sqrt(2)*sqrt(m)*((1/2*sqrt(4*z*(1-volt/(pulse+volt))*(pulse+volt)+2*m*v0^2-
4*v0*D*z*(1-volt/(pulse+volt))*(pulse+volt)/d1)-1/2*sqrt(2)*sqrt(m*v0^2))*d1/((1-
volt/(pulse+volt))*(pulse+volt))+(1/2*sqrt(4*z*(pulse+volt)+2*m*v0^2-4*v0*D*z*(1-
volt/(pulse+volt))*(pulse+volt)/d1)-1/2*sqrt(4*z*(1-
volt/(pulse+volt))*(pulse+volt)+2*m*v0^2-4*v0*D*z*(1-
volt/(pulse+volt))*(pulse+volt)/d1))*d2/volt)/z+1/2*L*sqrt(2)*sqrt(m/(z*(pulse+volt)
+1/2*m*v0^2-v0*D*z*(1-
volt/(pulse+volt))*(pulse+volt)/d1))+1/2*d3*sqrt(2)*sqrt(m/(z*(1-
volt/(pulse+volt))*(pulse+volt)+1/2*m*v0^2-v0*D*z*(1-
volt/(pulse+volt))*(pulse+volt)/d1))+1/2*sqrt(2)*sqrt(m*(z*(pulse+volt)+1/2*m*v0^2
-v0*D*z*(1-volt/(pulse+volt))*(pulse+volt)/d1))*L/(z*(pulse+volt))
>
```

Appendix C

For the determination of initial velocities for various MALDI ions, the data set of flight times vs. delay for given parameters of voltages, distances, and ion masses etc, was fitted to the theoretical value of flight times vs. delay, and the fit with the best chi squared value was then picked out as the initial velocity of the ion. The initial velocity parameter was varied by 10m/s increments over a range typically more than 1000 m/s . The C program used with some sample parameters is given below.

```
#include <stdio.h>
#include <math.h>
#include <strings.h>


double gDATAX[200],gDATAY[200];
long gPoints;

int read_file();
double TOF_monty(double offset,double vfinal,double Delay, double tau);
double TOF(double pulse, double v0, double D);
double chi(double a,double b,double c);

int main()
{
        read_file();

        double vfinal;
        double offset;
```

```
double vfinal_best,offset_best;
double best=10000;
double w;


double v1=-200;
double v2=200;
double offinc=10;

double vfinal_min=400;
double vfinal_max=1200;
double vel_inc=10;
FILE *foo;

double tau_best;
double tau_init=25;
double tau_final=25;
double tau;

foo=fopen("chis","w");

/* printf("starting brute force...\n");
printf("brute: %lf\n",1e9*TOF_monty(0,1000,0));
return 0; */

for (tau=tau_init;tau<=tau_final;tau=tau+50)
{
for (offset=v1;offset<=v2;offset=offset+offinc)
{
        printf("----> cycling %lf\n",offset);
        for (vfinal=vfinal_min;vfinal<=vfinal_max;vfinal=vfinal+vel_inc)
        {
                w=chi(offset,vfinal,tau);
                fprintf(foo,"%lf %lf %lf -> %10.8lf\n",offset,vfinal,tau,w);
                if (w<best)
                {
                        best=w;
                        vfinal_best=vfinal;
                        offset_best=offset;
                        tau_best=tau;
                }
                printf(". %lf\n",vfinal);
        }
}
```

```
        }
        fclose(foo);
bestest:

        printf("best fit: V: %lf   v0: %lf  tau: %lf\n",offset_best,vfinal_best,tau_best);
        FILE *fp;

        int i;
        long a1,a2;

        double x01,x02,x03;
        x01=offset_best;
        x02=vfinal_best;
        x03=tau_best;

        fp=fopen("best","w");
        for (i=0;i<=gPoints;i++)
        {
                w=TOF_monty(x01,x02,gDATAX[i],x03);
                w=TOF_monty(x01,x02,gDATAX[i],x03);

                a1=(long) (gDATAX[i]*1e9);
                a2=(long) (w*1e9);
                fprintf(fp,"%ld\t%ld\n",a1,a2);
        }
        fclose(fp);

        printf("write out %ld points\n",i);

        printf("## end of program\n");

}

// read in file
int read_file()
{
        FILE *fp;
        double v1,v2;

        int idx=0;

        fp=fopen("lue","r");
        if (fp==0)
        {
```

```
		printf("file not found!");
		return -1;
	}

	while (fscanf(fp,"%lf %lf",&v1,&v2)!=EOF)
	{
		gDATAX[idx]=v1*1e-9;
		gDATAY[idx]=v2*1e-9;
		idx++;
	}
	fclose(fp);
	gPoints=idx-1;
	printf("read in %ld points\n",gPoints);
	return 0;

}

// compute chi squared
double chi(double a,double b,double c)
{
	double chi1=0;
	double trial;
	int i;

	for (i=0;i<=gPoints;i++)
	{
	//trial=TOF(a,b,gDATAX[i]);
	trial=TOF_monty(a,b,gDATAX[i],c);
	chi1=chi1+(trial-gDATAY[i])*(trial-gDATAY[i])/(gDATAY[i]*gDATAY[i]);
	}

	if (chi1>1) return 1;
	return chi1;
}

// compute TOF using equations
double TOF(double offset, double v0, double D)
{
	double z,m,L,d1,d2,d3,volt,mirrorV,pulse;
	double U,G,E1,E2,E3;
	double T0,T1,T2;
	double t,t3,t4,t5;
	double tve;
```

```
        z=1.602e-19;
        m=726*1.66e-27;
        L=1.2126;
        d1=.006223;
        d2=.009474;
        d3=.001994;
        volt=17000;
        mirrorV=U*1.151;
        pulse=3000;

        U=pulse+volt;
        G=volt/U;

        E1=(1-G)*U/d1;
        E2=G*U/d2;
        E3= 4*U/L;

        T0=.5*m*v0*v0;
        T2=z*U+.5*m*v0*v0-v0*D*z*E1;
        T1=z*(1-G)*U+.5*m*v0*v0-v0*D*z*E1;

        double tp1,tp2,tp3;

        tp1=sqrt(2*m)/z;
        tp2=sqrt(T1)-sqrt(T0);
        tp3=sqrt(T2)-sqrt(T1);

        t=tp1*((tp2/E1)+(tp3/E2));
        t4=d3*sqrt(m/(2*T1));
        t3=L*sqrt(m/(2*T2));
        t5=2*sqrt(2*m*T2)/(z*E3);
        tve=t+t3+t4+t5+offset*1e-9;

        if (tve<0 || tve>1e-2) return 0;

        return tve;
}


// compute tof using brute force
double TOF_monty(double offset,double vfinal,double Delay,double tau)
{
        double z,m,L,d1,Ltot,d2,d3,dmirror,volt,mirrorV;
        double t,x,deltee,vx,vmax;
```

```
double gap,tve;
double ax,Vdrive,cvt,axm;
double pulse;
double t_mirror;
//double tau;

z=1.602e-19;
m=5734*1.66e-27;
L=1.16322;
d1=.006223;
d3=.009474; // was d2
d2=.001994; // was d3
volt=17000;
dmirror=.349;
mirrorV=volt+pulse;
Ltot=1.2126;
pulse=3000;
tau=tau*1e-9;


t=0; deltee=.3e-9;
x=0; vx=vfinal;
double gap_prev=d1;
double t_prev=0;

while (x<d1+d2+d3)
{
        if (x<=d1+d2+d3 && x>d1+d2) { gap=d3; }
        if (x<=d1+d2 && x>d1) { gap=d2; }
        if (x<=d1) { gap=d1; }

// no pulse
        if (t<=Delay) { Vdrive=0; }

// pulse
        if (t>Delay) { Vdrive=pulse;  }


// not field free (with penetration) between grids
        if (x>d1) { Vdrive=volt*0.0062; }

// towards ground
        if (x>d1+d2) { Vdrive=volt; }
```

```
            cvt=z/(m*gap);
            ax=Vdrive*cvt;

            x=x+vx*deltee+.5*ax*deltee*deltee;
            //if (vx<=vfinal)
            //{
            //        vx=vfinal*(1-exp(-t/tau));
            //}
            vx=vx+deltee*ax;
            t=t+deltee;
        //towards mirror
        }

        vmax=vx;

        tve=t+Ltot/vx;


        t_mirror=0; deltee=.4e-9;

        // in mirror
        axm=-mirrorV*z*1.151/(m*dmirror);
        while (vx>0)
        {
           vx=vx+axm*deltee;
           t_mirror=t_mirror+deltee;
        }
        tve=tve +2*t_mirror ;
        tve=tve - Delay +offset*1e-9;


        return tve ;
}
```